STIF

NASA Technical Memorandum 100013

(NASA-TM-100013) LIFT DISTRIBUTION AND VELOCITY FIELD MEASUREMENTS FOR A THREE-DIMENSIONAL, STEADY BLADE/VORTEX INTERACTION (NASA) 39 p CSCL 01A

N88-14962

Unclas
G3/02 0118108

Lift Distribution and Velocity Field Measurements for a Three-Dimensional, Steady Blade/Vortex Interaction

Stephen E. Dunagan and Thomas R. Norman

November 1987

National Aeronautics and
Space Administration

NASA Technical Memorandum 100013

Lift Distribution and Velocity Field Measurements for a Three-Dimensional, Steady Blade/Vortex Interaction

Stephen E. Dunagan,
Thomas R. Norman, Ames Research Center, Moffett Field, California

November 1987

National Aeronautics and
Space Administration

Ames Research Center
Moffett Field, California 94035

SUMMARY

A wind tunnel experiment simulating a steady three-dimensional helicoptor rotor blade/vortex interaction is reported. The experimental configuration consisted of a vertical semispan vortex-generating wing, mounted upstream of a horizontal semispan rotor blade airfoil. A three-dimensional laser velocimeter was used to measure the velocity field in the region of the blade. Sectional lift coefficients were calculated by integrating the velocity field to obtain the bound vorticity. Total lift values, obtained by using an internal strain-gauge balance, verified the laser velocimeter data. Parametric variations of vortex strength, rotor blade angle of attack, and vortex position relative to the rotor blade were explored. These data are reported herein (with attention to experimental limitations) to provide a dataset for the validation of analytical work.

NOMENCLATURE

c	blade chord
c_l	sectional lift coefficient, L/qc
s	vortex-circulation box-side dimension
Tol_v	experimental uncertainty in cross-stream velocity mean
Tol_w	experimental uncertainty in vertical velocity mean
u	streamwise velocity component
u_∞	free-stream velocity
v	cross-stream velocity component
w	vertical velocity component
x	streamwise coordinate
y	cross-stream coordinate
z	vertical coordinate
α_b	blade angle of attack
α_{vg}	vortex-generating wing angle of attack
σ_v	standard deviation of v velocity
σ_w	standard deviation of w velocity
θ_t	blade twist angle

INTRODUCTION

Blade/vortex interactions (which occur as the tip vortex trailed by a lifting rotor blade passes near the following blade) play an important role in determining the acoustic and aerodynamic environment surrounding the rotor. Such interactions may be described as parallel (two-dimensional, unsteady) or perpendicular (three-dimensional (3-D), steady). Additionally, a broad variety of 3-D unsteady oblique interactions is possible. The 3-D steady interaction occurs in hover when wake contraction places tip vortices in close proximity to following blades. The vorticity vector of the tip vortex is perpendicular to the blade, establishing a complex 3-D flow field. The effect of the vortex on the aerodynamic field surrounding the blade may be quite pronounced.

This paper describes an experimental investigation of a 3-D steady blade-vortex interaction. The experimental configuration consisted of a semispan wing (blade) located near the path of the tip vortex shed from an upstream vortex-generating wing. Aerodynamic data obtained nonintrusively with a 3-D laser velocimeter (LV) and with an internal strain-gage balance are presented. Velocity measurements of the circulation around the blade were used to calculate spanwise blade lift distributions with high spatial resolution and versatility. Mean-flow velocities were also measured over grids located upstream of the blade. Variations of vortex strength, vortex position, and blade angle of attack were examined.

This report has been compiled to provide theoreticians with a data set for validation purposes. A correlation of these data with panel method (VSAERO) predictions for this flow may be found in reference 1. The experimental techniques described in this report may be of interest to those doing an experimental examination of these or related phenomena. The data obtained in this study enhance understanding of the mechanisms of the 3-D steady blade-vortex interaction.

EXPERIMENTAL APPARATUS

Flow Facility

Testing was conducted in the 7- by 10-Foot Subsonic Wind Tunnel at NASA Ames Research Center. This is a continuous-operation, closed-loop facility capable of test section velocities in the range of 0 to 160 m/sec (dynamic pressures from 0 to 5.74 kPa). The flow was regulated to provide a dynamic pressure of 2.2 kPa $\pm 2\%$ (free-stream velocity, u_∞, of approximately 60 m/sec) in the test section. The Reynolds number based on semispan blade-airfoil chord was 850,000 and the Mach number was 0.17. The flow quality was limited by streamwise turbulence levels of approximately 2% in the test section.

Model

The model geometry is shown in figures 1 and 2. A semispan wing representing the following blade in the blade-vortex interaction was mounted horizontally in the test section. A Boeing V23010-1.58 airfoil with 0.2091-m chord (c) and 1.524-m span was selected. This blade was designed with twist (θ_t) along its span to simulate the nonuniform spanwise loading of a twisted full-scale rotor. Table 1 provides data for the airfoil section coordinates and twist distribution. Mounting apparatus permitted adjustment of the blade angle of attack (α_b). All blade angle values reported were measured at a y/c location 2.065.

A splitter plate was used to minimize the effects of the wall boundary layer; it reduced the effective span to 1.076 m. This span included a 0.4318-m blade tip which was mounted to the inboard blade section by means of a six-component internal strain-gage balance, which permitted measurement of total lift for the tip. The coordinate system for this study is right-hand orthogonal with streamwise (x, positive downstream), cross-stream (y, positive to the left when facing downstream), and vertical (z, positive up) unit vectors. The origin was located at the leading edge of the blade tip on the blade chord line. The velocities u, v, and w correspond to the x, y, and z directions.

A vortex-generating (V-G) wing (NACA 0018 airfoil section, 0.2032-m chord, nominally 1.067-m span) was mounted vertically from the wind tunnel ceiling with its trailing edge 0.5144 m upstream of the leading edge of the blade. The mounting apparatus was designed to permit adjustment of the wing position in the cross-stream and vertical directions as well as wing angle of attack (α_{vg}). This allowed the mean location of the convected V-G wing-tip vortex to be positioned relative to the blade. The rather close streamwise spacing of the V-G wing and the blade did not provide a fully rolled up vortex in the interaction region. However, unsteadiness of the vortex position in the y and z directions made it necessary to limit this spacing to obtain a more steady interaction.

A feature of this experimental configuration is the presence of the V-G wing viscous wake in the interaction region. This could have been avoided by locating the V-G wing below the blade or moving the blade to the opposite wall. However, test scheduling and wind tunnel structural limitations did not permit the use of such a configuration in this study. The effect of this wake is apparent in the test data, particularly in the blade loading distributions, where a localized loss of lift (due to the wake velocity deficit) can be seen.

Instrumentation

A coupled, 3-D, zoom, confocal-backscatter L-V system was used to obtain velocity data. Streamwise and vertical velocity components were measured directly. The cross-stream component was resolved from a third strongly coupled channel having coupling angles from 10 deg to 28 deg, depending on the cross-stream location. Zoom optics provided cross-stream probe volume translation on both the orthogonal and coupled channels. Bragg cells were used to introduce a frequency bias to resolve velocity sign ambiguity. Confocal-backscatter collection provided good alignment stability. Low signal-to-noise ratios characteristic of long-range (1.1 to 3.3 m) backscatter operation made it necessary to frequency down-mix the photomultiplier tube signal and narrow-band filter before analysis with conventional counter processor units. All LV system functions were automated for computer control, including software control of sample size to obtain a specified velocity confidence interval (95% confidence, ± 0.1 m/sec). The flow was seeded with a polydispersed mineral oil aerosol. The seed was injected downstream of the test section to permit heavier particles to settle out (in the tunnel circuit) before passing through the probe volume. Previous studies[2,3] using this instrument have indicated the suitability of this configuration for mean velocity measurement, particularly for the orthogonal channels.

The LV was used to obtain three types of data. In one mode the probe volume was traversed to specified points on a rectangular grid defining a $y-z$ plane. Measurements of the three velocity components were recorded, which provided documentation of the flow over a large field. In the second mode, the probe volume was traversed in a rectangular path in the $x-z$ plane which encompassed the blade. Streamwise velocity components were recorded at 11 evenly spaced points along the horizontal traverses; vertical components were recorded at 7 points along the vertical paths. This permitted a calculation of the sectional lift from an evaluation of the line integral of the tangential velocity around the closed path.[4] In the third mode, a similar line-integral approach was used to evaluate the circulation internal to a rectangular path in the $y-z$ plane encompassing the vortex.

Additionally, the LV laser was used as the source of illumination for laser-light sheet-flow visualization. The laser output was redirected through cylindrical optics to form a $y-z$ planar light sheet. Mineral oil mist was also used as the scattering media for flow visualization. Forward scattered light (at a scattering angle of 30 deg) was imaged and recorded with a video camera. Strong inertial effects in the vortex core greatly reduced seed concentration, making the core stand out as a dark spot in the field of scattered light. This permitted the measurement of both the vortex position and the vortex unsteadiness.

A six-component internal strain-gage balance attached the outboard 0.4318-cm blade tip section to the blade root. This permitted an independent measurement of lift for verification of the LV data. Additional instrumentation provided test-section dynamic and static pressure and total-temperature measurements.

TEST CONFIGURATIONS

The effects of variations in vortex strength, vortex position and blade angle of attack on the blade lift distribution were examined in this test. Table 2 lists the various configurations studied and the types of data obtained. Configuration 1 data, obtained in a previous study (Norman, T. R., and Dunagan, S. E., 1987, NASA Ames Research Center, NASA-TM, to be published) without the V-G wing, are presented here as the no-interaction baseline case for $\alpha_b = 6.67$ deg. Configuration 2 is intended to be representative of a physically realistic, hovering, 3-D, steady blade-vortex interaction. The vortex is shed from a V-G wing of a similar chord and angle of attack as the blade. The vortex position was selected after examining experimental shadowgraph data[5] obtained for a four-bladed rotor in hover. Configurations 3, 4, and 5 represent single-point variations of vortex strength, vortex position, and blade angle of attack, respectively, and configuration 6 provides the no-interaction baseline case for $\alpha_b = 3.33$ deg. For configuration 6, the interaction was effectively eliminated by reducing the V-G wing angle of attack to zero and locating the wing tip well above the blade.

RESULTS

Flow Visualization

Vortex position and unsteadiness were accurately determined for one orientation of the V-G wing (configuration 2) by using the laser-light sheet flow visualization technique described in the instrumentation section. Mean y/c and z/c locations for configuration 2 were found to be 0.95 and -0.51, respectively. Standard deviations were measured as 0.015 and 0.028, respectively.

Velocity Grids

Three-dimensional velocity data were obtained over spatial grids defining $y-z$ planes at an x-location 0.75 chord upstream of the blade leading edge. These data were useful in two ways. Large grids that covered the entire region of interest were obtained for use in identifying the effect of the V-G wing on the flow approaching the blade. Additionally, smaller grids provide a detailed picture of the vortex velocity field. Figures 3 through 9 present large and small velocity grid data for configurations 2 and 3, and large velocity grid data for configurations 4 and 5. These same data are also listed in tables 3 through 9. All velocity data have been normalized by the free-stream velocity.

Spanwise Lift Coefficients

The primary objective of the study was the acquisition of spanwise blade lift coefficient (c_l) distributions for the various configurations. These were obtained by integrating the tangential velocity over a closed path (box) around the blade (in the $x-z$ plane) to obtain the bound vorticity. Figure 10 gives the geometry of the circulation box used in this study. The Kutta-Joukowski theorem was used to equate this vorticity to sectional lift. Experimental data for lift distribution for all the configurations tested are listed in table 10 and presented graphically in figure 11.

These distributions show the detailed effects of the vortex and V-G wing wake. The upward velocities induced by the vortex outboard of the vortex center increase the local angle of attack for flow over the outboard end of the tip, which increases the lift. A corresponding decrease in lift may be observed inboard of the vortex center. Additionally, the velocity deficit of the V-G wing wake is responsible for the localized loss of lift observed at y/c locations near 1.25.

Vortex Circulation

In a similar manner, the integration of the tangential velocity around a closed path (in the $y-z$ plane) encompassing the viscous core of the vortex was used to measure the vortex strength. The calculated vorticity from square and rectangular (aspect ratio = 1.2) boxes was averaged to get the vortex circulation values presented in figure 12. Vortex circulation is plotted as a function of the short-side dimension (s) for configurations 2 and 3.

For a fully "rolled up" vortex, one would expect to see a leveling of vortex strength as the box perimeter fully encompassed the viscous vortex core. This trend is not observed in these data, which indicates that additional vorticity from the blade wake is contained in the larger boxes. The extension of box size to much larger dimensions would have reduced the measured velocity to values on the order of the resolution limit of the LV and thus would have degraded the quality of the measurement. These results point out the limitation of this method for quantifying the strength of tip vortices in the near field of a lifting wing.

Total Lift

To provide a means of checking the reliability of lift distribution data obtained from the laser velocimeter, total lift data for the tip section of the blade were obtained from an internal strain-gage balance. The tip section was separated from the blade root by a gap of 0.1 inches to permit the balance to operate freely. To avoid the localized loss of lift near this gap, a thin layer of tape was applied to the wing surface spanning the junction. Balance lift coefficient data for each configuration tested, for both the sealed and open gap, are presented in table 11. Average and standard deviation values are listed at the bottom. A correction (discussed in the error analysis section) was applied to these average lift coefficient values.

Finally, the LV lift coefficient distributions were integrated over the tip span to obtain a total lift coefficient for the tip section. Both the corrected average lift coefficients and the integrated LV values are also reported at the bottom of table 11. Lift coefficient values agree within 3% for all configurations tested.

ERROR ANALYSIS

The usefulness of these data for correlation and validation purposes is limited by the systematic and random sources of error present in each type of data obtained. The following paragraphs are dedicated to the description and quantification of such errors.

Wall Effects

These data obtained for flow in a rectangular duct 2.134 m high by 3.048 m wide (model origin on tunnel axis) will differ from predictions computed for free-stream flow because of the effects of the wind tunnel walls. In particular, the image vortex system introduced by the walls has a marked effect on the blade lift distribution.[1] To account for the effect of the tunnel walls on the lift data, a downwash correction is suggested.[6] Blade and V-G wing angles may be corrected to obtain an effective angle of attack to be used in the computational model.

Velocity Data

Two systematic error sources associated with the LV data have been identified. The first is related to the drift in the rather complex 3-D zoom calibration of the instrument during the test. In order to quantify this error, a post-test calibration of the instrument was taken at the completion of the test. Velocity data reduced by using the pre- and post-test calibrations were compared. Table 12 presents the average velocity error (normalized by u_∞) for each velocity component, computed for each of the velocity grid data files reported. A graphic presentation of this calibration drift error for the large configuration 2 grid is presented in figure 13. It is clear that the cross-stream component suffers most from this source of error (owing to the small coupling angle used in this system).

Calibration drift is a possible source of error for the lift distribution data also, though the absence of any cross stream component measurement from the circulation computation reduces its impact. A comparison of sectional lift coefficient measurements computed with the pre- and post-test calibrations for each of the lift coefficient measurements of configuration 2 indicates a maximum error due to calibration drift of 0.2%

The second systematic error found in the LV data relates to deflection of the blade with lift. The strain-gage balance attachment of the blade tip to the blade root was somewhat elastic and permitted flection in the vertical direction. To quantify this error, deflections were measured optically at both the blade tip and the tip-root junction using the vertical translator of the LV. Ten deflection measurements were averaged to obtain the mean deflection values reported in table 13. A rigorous comparison with a predicted velocity field may require a correction to vertical blade position, with the blade root modeled as a cantilevered beam and the tip-root attachment approximated by a pinned connection.

Random error associated with turbulent flow was treated statistically with data reduction software. A desired velocity tolerance of 0.1 m/sec was specified at the beginning of the experiment. Based on the continually updated variance of the data coming in, the data acquisition program computed the sample size required to obtain a sample mean within this tolerance of the true population mean with 95% confidence. In highly turbulent regions, the required sample size became very large and it was necessary to limit the number of samples because of time restraints. An upper limit of 2000 was placed on the sample size. To document the statistical reliability of these data, the experimental uncertainty in normalized mean velocity is listed in tables 3 through 9, along with the nominal sample size.

Because of the low coupling angle of the LV system, one expects much higher turbulence levels on the resolved cross-stream velocity component compared to the directly measured vertical component.[2] This trend may be seen in these data as well as in previous studies, and emphasizes the inability of this optical configuration to correctly resolve the cross-stream turbulence or the various stress tensor components derived from it.

Narrow filter bandwidths are required to process the noisy signal obtained from long range backscatter. Occasionally these bandwidths are insufficient to contain the data scatter caused by real turbulence, giving rise to another random error source. Care is taken during the test to avoid this condition. However, for highly turbulent regions, such as the core of a vortex or a turbulent wake, the situation is unavoidable. These data must be regarded with skepticism. For this reason the vortex core data has been omitted from all the velocity grids.

Flow Visualization

Systematic errors associated with the flow visualization setup were not evaluated. The random error owing to flow induced vortex positional unsteadiness was treated in the standard statistical fashion. The true mean y/c and z/c positions for configuration 2 are within ± 0.005 and 0.010 of the previously reported mean values with 95% confidence.

Balance Data

For this study a three-quarter inch internal strain-gage balance designed to be mounted longitudinally in the flow was adapted to mount transversely in the model at the airfoil lifting center (quarter-chord). The static pitching moment owing to the weight of the tip made it impossible to balance the pitching moment gage (which was designed to encounter only limited rolling moments). While this gage was not critical for the desired lift measurement, lift coefficient data were affected via the interactions equations used to convert balance voltages to loads. A first-order correction for this error was determined by placing known weights on the blade tip and computing a simple multiplier coefficient. These corrected data are tabulated at the bottom of table 11.

Assuming that random errors are reflected in the variance of lift coefficient values listed in table 11, it may be said with 95% confidence that the true means lie within the range defined by the sample average, plus or minus the sample tolerance.

SUMMARY OF RESULTS

An experimental investigation of the 3-D steady blade-vortex interaction has been conducted. The effects of variations of vortex strength, vortex position, and blade angle of attack on spanwise lift have been examined. Flow velocity data have been obtained to characterize the incident vortex. Detailed blade lift distribution data have been acquired nonintrusively using laser velocimeter instrumentation. Total-lift measurements obtained from an internal strain-gage balance provide added confidence in the LV results.

All data acquired during the test have been presented. Velocity grid data identify the character of the vortex and residual V-G wing wake entering the interaction region. Lift distribution data provide a spatially detailed view of the effect of the interaction on lift, including localized loss of lift resulting from the V-G wing wake. Significant error sources for all of the data presented have been identified and quantified.

REFERENCES

[1] Dunagan, S. E.; and Norman, T. N.: Lift Distributions for a 3-Dimensional Steady Blade-Vortex Interaction. Proceedings, American Helicopter Society National Specialists' Meeting on Aerodynamics and Aeroacoustics, Arlington, Texas, Feb, 1987.

[2] Orloff, K. L.; and Snyder, P. K.: Laser Doppler Anemometer Measurements Using Nonorthogonal Velocity Components: Error Estimates. Applied Optics, 21(2), Jan. 1982.

[3] Snyder, P. K.; Orloff, K. L.; and Aoyagi, K.: Performance and Analysis of a Three-Dimensional Nonorthogonal Laser Doppler Anemometer. NASA TM 81283, 1981.

[4] Orloff, K. L.: Spanwise Lift Distributions on a Wing from Flowfield Velocity Surveys. J. of Aircraft, 17(12), Dec. 1980, p. 875.

[5] Norman, T. R.; and Light, J. S.: Rotor Tip Vortex Geometry Measurements Using the Wide-Field Shadowgraph Technique. AIAA Paper 86-1780 CP, AIAA 4th Applied Aerodynamics Conference, San Diego, CA, June 1986.

[6] Rae, Wm H., Jr.; and Pope, A.: Low Speed Wind Tunnel Testing, 2nd ed., John Wiley & Sons, New York, 1984, p. 383.

TABLE 1. - BLADE AIRFOIL COORDINATES AND TWIST DISTRIBUTION

Airfoil coordinates

x/c	lower surface z/c	upper surface z/c
0.000	-0.0225	-0.0225
0.005	-0.0329	-0.0078
0.010	-0.0362	-0.0024
0.015	-0.0378	0.0019
0.025	-0.0394	0.0096
0.035	-0.0404	0.0155
0.047	-0.0412	0.0214
0.060	-0.0420	0.0265
0.080	-0.0434	0.0327
0.110	-0.0449	0.0396
0.150	-0.0471	0.0455
0.190	-0.0494	0.0489
0.230	-0.0513	0.0499
0.270	-0.0522	0.0499
0.310	-0.0522	0.0497
0.350	-0.0517	0.0490
0.390	-0.0505	0.0480
0.430	-0.0487	0.0465
0.470	-0.0468	0.0446
0.510	-0.0440	0.0424
0.550	-0.0412	0.0397
0.590	-0.0380	0.0369
0.630	-0.0346	0.0336
0.670	-0.0308	0.0301
0.710	-0.0269	0.0263
0.750	-0.0226	0.0223
0.790	-0.0182	0.0181
0.830	-0.0136	0.0137
0.870	-0.0093	0.0093
0.910	-0.0057	0.0056
0.945	-0.0031	0.0028
0.960	-0.0024	0.0024
1.000	-0.0000	0.0000

Twist distribution

y/c	θ_t,deg
0.000	-0.338
1.000	-0.119
2.000	-0.004
2.065	0.000
3.000	0.003
4.000	-0.094
5.000	-0.298
6.000	-0.607
7.000	-1.022
7.288	-1.159

TABLE 2. - TEST MATRIX

	Configuration 1	2	3	4	5	6
Blade angle of attack, α_b, deg	6.56	6.67	6.67	6.67	3.33	3.33
V-G wing angle of attack, α_{vg}, deg	-	6	9	6	6	0
Cross stream vortex position, y/c	-	1.00	1.00	1.00	1.00	1.00
Vertical vortex position, z/c	-	-0.50	-0.50	-0.25	-0.50	3.00
Types of data obtained						
Velocity grid of blade inflow		x	x	x	x	
Blade lift distributions	x	x	x	x	x	x
Vortex circulation		x	x			
Strain gage balance lift	x	x	x	x	x	x
Laser light sheet flow visualization		x				

TABLE 3. - LARGE VELOCITY GRID DATA, CONFIGURATION NUMBER 2

	y/c	z/c	v	w	σ_v	σ_w	Tol_v	Tol_w	N
1	-0.5033	-0.9999	0.0303	0.0184	0.0489	0.0091	0.0068	0.0013	200
2	-0.5033	-0.7498	0.0248	0.0188	0.0629	0.0140	0.0087	0.0020	200
3	-0.5033	-0.4997	0.0371	0.0274	0.0386	0.0078	0.0076	0.0015	100
4	-0.5033	-0.2498	0.0174	0.0290	0.0602	0.0138	0.0083	0.0019	200
5	-0.5033	0.0003	0.0173	0.0448	0.0408	0.0085	0.0080	0.0017	100
6	-0.5033	0.2501	0.0322	0.0218	0.0354	0.0068	0.0070	0.0013	100
7	-0.5033	0.5001	0.0327	0.0357	0.0701	0.0147	0.0079	0.0017	300
8	-0.2521	-1.0002	0.0182	0.0259	0.0522	0.0110	0.0072	0.0015	200
9	-0.2521	-0.7502	0.0221	0.0226	0.0631	0.0151	0.0072	0.0017	300
10	-0.2521	-0.5001	0.0275	0.0277	0.0578	0.0121	0.0066	0.0014	300
11	-0.2521	-0.2501	0.0258	0.0364	0.0377	0.0075	0.0074	0.0015	100
12	-0.2521	-0.0001	0.0135	0.0431	0.0639	0.0131	0.0073	0.0015	300
13	-0.2521	0.2498	0.0302	0.0307	0.0564	0.0131	0.0079	0.0018	200
14	-0.2521	0.5001	0.0402	0.0222	0.0478	0.0090	0.0066	0.0012	200
15	-0.0010	-1.0001	0.0118	0.0295	0.0558	0.0112	0.0063	0.0013	300
16	-0.0010	-0.7498	0.0092	0.0369	0.0484	0.0089	0.0067	0.0012	200
17	-0.0010	-0.4997	0.0115	0.0394	0.0422	0.0083	0.0059	0.0012	200
18	-0.0010	-0.2497	0.0262	0.0441	0.0616	0.0134	0.0070	0.0015	300
19	-0.0010	0.0003	0.0289	0.0465	0.0516	0.0092	0.0072	0.0013	200
20	-0.0010	0.2501	0.0331	0.0435	0.0583	0.0121	0.0066	0.0014	300
21	-0.0010	0.5001	0.0496	0.0346	0.0559	0.0119	0.0077	0.0017	200
22	0.2501	-1.0002	0.0017	0.0364	0.0498	0.0089	0.0069	0.0013	200
23	0.2501	-0.7502	0.0263	0.0336	0.0607	0.0116	0.0069	0.0013	300
24	0.2501	-0.5001	0.0127	0.0502	0.0539	0.0099	0.0075	0.0014	200
25	0.2501	-0.2501	0.0213	0.0515	0.0530	0.0107	0.0074	0.0015	200
26	0.2501	-0.0001	0.0394	0.0489	0.0755	0.0156	0.0074	0.0015	400
27	0.2501	0.2498	0.0599	0.0486	0.0510	0.0101	0.0071	0.0014	200
28	0.2501	0.5001	0.0668	0.0328	0.0557	0.0122	0.0078	0.0017	200
29	0.5017	-1.0001	-0.0198	0.0337	0.0654	0.0131	0.0074	0.0015	300
30	0.5017	-0.7498	0.0168	0.0418	0.0557	0.0104	0.0077	0.0015	200
31	0.5017	-0.4997	0.0061	0.0685	0.0507	0.0098	0.0071	0.0014	200
32	0.5017	-0.2497	0.0301	0.0737	0.0552	0.0104	0.0077	0.0015	200
33	0.5017	0.0003	0.0438	0.0574	0.0547	0.0107	0.0076	0.0015	200
34	0.5017	0.2501	0.0544	0.0552	0.0693	0.0135	0.0079	0.0015	300
35	0.5017	0.5001	0.0504	0.0414	0.0606	0.0118	0.0069	0.0014	300
36	0.7528	-1.0002	-0.0304	0.0286	0.0678	0.0119	0.0077	0.0014	300
37	0.7528	-0.7502	-0.0263	0.0630	0.0482	0.0087	0.0067	0.0012	200
38	0.7528	-0.5001	0.0174	0.1134	0.0709	0.0142	0.0080	0.0016	300
39	0.7528	-0.2501	0.0550	0.0852	0.0727	0.0133	0.0082	0.0015	300
40	0.7528	-0.0001	0.0675	0.0651	0.0685	0.0128	0.0078	0.0015	300
41	0.7528	0.2498	0.0887	0.0475	0.0555	0.0103	0.0077	0.0014	200
42	0.7528	0.5001	0.0510	0.0501	0.0744	0.0138	0.0073	0.0014	400
43	1.0041	-1.0001	-0.0541	0.0062	0.0673	0.0127	0.0077	0.0015	300
44	1.0041	-0.7498	-0.0952	0.0217	0.0742	0.0119	0.0073	0.0012	400
45	1.0041	-0.2497	0.0759	0.0640	0.0740	0.0125	0.0084	0.0014	300
46	1.0041	0.0003	0.0809	0.0661	0.0701	0.0137	0.0079	0.0016	300
47	1.0041	0.2501	0.0597	0.0596	0.0674	0.0126	0.0076	0.0014	300
48	1.0041	0.5001	0.0726	0.0492	0.0545	0.0109	0.0076	0.0015	200
49	1.2545	-1.0002	-0.0462	-0.0112	0.0688	0.0107	0.0078	0.0012	300
50	1.2545	-0.7501	-0.0540	-0.0487	0.0820	0.0150	0.0072	0.0013	500

TABLE 3. - CONCLUDED

	y/c	z/c	v	w	σ_v	σ_w	Tol_v	Tol_w	N
51	1.2545	-0.5001	-0.0216	-0.1021	0.0772	0.0152	0.0076	0.0015	400
52	1.2545	-0.2501	0.0376	-0.0694	0.0756	0.0152	0.0074	0.0015	400
53	1.2545	-0.0001	0.0243	-0.0246	0.1393	0.0286	0.0079	0.0016	1200
54	1.2545	0.2498	0.0679	-0.0107	0.1100	0.0221	0.0082	0.0016	700
55	1.2545	0.5001	0.0747	-0.0035	0.1091	0.0207	0.0076	0.0014	800
56	1.5032	-1.0001	-0.0219	-0.0251	0.0571	0.0099	0.0080	0.0014	200
57	1.5032	-0.7498	0.0086	-0.0445	0.0561	0.0095	0.0078	0.0013	200
58	1.5032	-0.4997	-0.0069	-0.0510	0.0708	0.0121	0.0070	0.0012	400
59	1.5032	-0.2497	0.0288	-0.0502	0.0738	0.0130	0.0073	0.0013	400
60	1.5032	0.0003	0.0443	-0.0282	0.0772	0.0137	0.0076	0.0014	400
61	1.5032	0.2501	0.0545	-0.0111	0.0753	0.0140	0.0074	0.0014	400
62	1.5032	0.5001	0.0645	-0.0032	0.0587	0.0101	0.0067	0.0011	300
63	1.7526	-1.0002	-0.0055	-0.0256	0.0718	0.0130	0.0071	0.0013	400
64	1.7526	-0.7501	0.0057	-0.0320	0.0716	0.0127	0.0081	0.0014	300
65	1.7526	-0.5001	0.0063	-0.0318	0.0565	0.0097	0.0079	0.0014	200
66	1.7526	-0.2501	0.0109	-0.0202	0.0710	0.0122	0.0070	0.0012	400
67	1.7526	-0.0001	0.0287	-0.0099	0.0686	0.0114	0.0078	0.0013	300
68	1.7526	0.2498	0.0352	-0.0025	0.0706	0.0127	0.0081	0.0015	300
69	1.7526	0.5001	0.0264	0.0048	0.0649	0.0107	0.0074	0.0012	300
70	2.0003	-1.0001	0.0129	-0.0223	0.0580	0.0098	0.0081	0.0014	200
71	2.0003	-0.7498	0.0069	-0.0209	0.0723	0.0121	0.0082	0.0014	300
72	2.0003	-0.4997	0.0075	-0.0205	0.0657	0.0114	0.0075	0.0013	300
73	2.0003	-0.2497	-0.0021	-0.0132	0.0864	0.0158	0.0076	0.0014	500
74	2.0003	0.0003	0.0229	-0.0056	0.0768	0.0139	0.0076	0.0014	400
75	2.0003	0.2501	0.0522	-0.0031	0.0779	0.0139	0.0069	0.0012	500
76	2.0003	0.5001	0.0401	-0.0001	0.0713	0.0127	0.0081	0.0014	300
77	2.2493	-1.0002	0.0191	-0.0217	0.0797	0.0138	0.0070	0.0012	500
78	2.2493	-0.7501	0.0089	-0.0166	0.0658	0.0108	0.0075	0.0012	300
79	2.2493	-0.5001	0.0209	-0.0166	0.0799	0.0143	0.0079	0.0014	400
80	2.2493	-0.2501	0.0341	-0.0117	0.0733	0.0122	0.0073	0.0012	400
81	2.2493	-0.0001	0.0420	-0.0043	0.0730	0.0128	0.0083	0.0015	300
82	2.2493	0.2498	0.0374	0.0031	0.0833	0.0137	0.0074	0.0012	500
83	2.2493	0.5000	0.0363	0.0046	0.0811	0.0139	0.0080	0.0014	400
84	2.4969	-1.0001	0.0153	-0.0183	0.0770	0.0127	0.0076	0.0013	400
85	2.4969	-0.7498	0.0261	-0.0173	0.0737	0.0130	0.0084	0.0015	300
86	2.4969	-0.4997	0.0229	-0.0092	0.0834	0.0137	0.0083	0.0014	400
87	2.4969	-0.2497	0.0294	-0.0057	0.0896	0.0146	0.0079	0.0013	500
88	2.4969	0.0003	0.0298	0.0037	0.0883	0.0148	0.0078	0.0013	500
89	2.4969	0.2501	0.0307	0.0087	0.0806	0.0127	0.0071	0.0011	500
90	2.4969	0.5001	0.0363	0.0080	0.0822	0.0130	0.0073	0.0012	500

TABLE 4. - LARGE VELOCITY GRID DATA, REPEAT CONFIGURATION NUMBER 2

	y/c	z/c	v	w	σ_v	σ_w	Tol_v	Tol_w	N
1	-0.5033	-0.9999	0.0141	0.0239	0.0495	0.0105	0.0069	0.0015	200
2	-0.5033	-0.7497	0.0260	0.0240	0.0522	0.0100	0.0073	0.0014	200
3	-0.5033	-0.4997	0.0200	0.0301	0.0496	0.0105	0.0069	0.0015	200
4	-0.5033	-0.2497	0.0283	0.0236	0.0529	0.0114	0.0073	0.0016	200
5	-0.5033	0.0003	0.0375	0.0272	0.0533	0.0102	0.0074	0.0014	200
6	-0.5033	0.2503	0.0454	0.0224	0.0446	0.0093	0.0062	0.0013	200
7	-0.5033	0.5003	0.0514	0.0235	0.0624	0.0136	0.0071	0.0016	300
8	-0.2521	-1.0003	0.0033	0.0229	0.0616	0.0123	0.0070	0.0014	300
9	-0.2521	-0.7502	0.0251	0.0256	0.0555	0.0110	0.0077	0.0015	200
10	-0.2521	-0.5002	0.0170	0.0385	0.0540	0.0115	0.0075	0.0016	200
11	-0.2521	-0.2502	0.0266	0.0325	0.0557	0.0109	0.0077	0.0015	200
12	-0.2521	-0.0002	0.0070	0.0394	0.0609	0.0129	0.0069	0.0015	300
13	-0.2521	0.2498	0.0485	0.0300	0.0615	0.0128	0.0070	0.0015	300
14	-0.2521	0.5001	0.0466	0.0260	0.0639	0.0141	0.0072	0.0016	300
15	-0.0010	-1.0002	0.0164	0.0261	0.0558	0.0114	0.0077	0.0016	200
16	-0.0010	-0.7497	0.0251	0.0331	0.0519	0.0103	0.0072	0.0014	200
17	-0.0010	-0.4997	0.0071	0.0400	0.0664	0.0137	0.0075	0.0016	300
18	-0.0010	-0.2497	0.0159	0.0453	0.0549	0.0109	0.0076	0.0015	200
19	-0.0010	0.0003	0.0368	0.0411	0.0613	0.0118	0.0069	0.0013	300
20	-0.0010	0.2503	0.0397	0.0421	0.0628	0.0121	0.0071	0.0014	300
21	-0.0010	0.5003	0.0464	0.0319	0.0592	0.0115	0.0067	0.0013	300
22	0.2501	-1.0003	0.0044	0.0275	0.0533	0.0106	0.0074	0.0015	200
23	0.2501	-0.7502	0.0141	0.0381	0.0591	0.0111	0.0067	0.0013	300
24	0.2501	-0.5002	0.0113	0.0491	0.0491	0.0095	0.0068	0.0013	200
25	0.2501	-0.2502	0.0198	0.0512	0.0536	0.0107	0.0074	0.0015	200
26	0.2501	-0.0002	0.0379	0.0534	0.0534	0.0097	0.0074	0.0014	200
27	0.2501	0.2498	0.0533	0.0471	0.0640	0.0132	0.0073	0.0015	300
28	0.2501	0.5001	0.0500	0.0381	0.0560	0.0103	0.0078	0.0014	200
29	0.5017	-1.0002	0.0006	0.0304	0.0592	0.0119	0.0067	0.0014	300
30	0.5017	-0.7497	0.0004	0.0524	0.0562	0.0101	0.0064	0.0012	300
31	0.5017	-0.4997	0.0146	0.0650	0.0653	0.0127	0.0074	0.0015	300
32	0.5017	-0.2497	0.0367	0.0655	0.0554	0.0105	0.0077	0.0015	200
33	0.5017	0.0003	0.0392	0.0616	0.0637	0.0125	0.0072	0.0014	300
34	0.5017	0.2503	0.0554	0.0535	0.0532	0.0107	0.0074	0.0015	200
35	0.5017	0.5003	0.0564	0.0456	0.0612	0.0110	0.0069	0.0013	300
36	0.7528	-1.0003	-0.0233	0.0237	0.0520	0.0091	0.0072	0.0013	200
37	0.7528	-0.7502	-0.0345	0.0607	0.0548	0.0106	0.0076	0.0015	200
38	0.7528	-0.5002	0.0050	0.1080	0.0651	0.0121	0.0074	0.0014	300
39	0.7528	-0.2502	0.0505	0.0804	0.0712	0.0129	0.0070	0.0013	400
40	0.7528	-0.0002	0.0568	0.0681	0.0669	0.0120	0.0076	0.0014	300
41	0.7528	0.2498	0.0739	0.0598	0.0577	0.0113	0.0080	0.0016	200
42	0.7528	0.5001	0.0563	0.0490	0.0620	0.0118	0.0070	0.0013	300
43	1.0041	-1.0002	-0.0363	0.0054	0.0707	0.0130	0.0069	0.0013	400
44	1.0041	-0.7497	-0.0940	0.0208	0.0722	0.0113	0.0071	0.0011	400
45	1.0041	-0.2497	0.0837	0.0650	0.0805	0.0144	0.0079	0.0014	400
46	1.0041	0.0003	0.0662	0.0629	0.0841	0.0144	0.0074	0.0013	500
47	1.0041	0.2503	0.0624	0.0571	0.0885	0.0153	0.0078	0.0014	500
48	1.0041	0.5003	0.0720	0.0475	0.0692	0.0118	0.0078	0.0013	300
49	1.2545	-1.0003	-0.0352	-0.0165	0.0787	0.0130	0.0078	0.0013	400
50	1.2545	-0.7501	-0.0427	-0.0415	0.0903	0.0162	0.0079	0.0014	500

TABLE 4. - CONCLUDED

	y/c	z/c	v	w	σ_v	σ_w	Tol_v	Tol_w	N
51	1.2545	-0.5002	-0.0050	-0.0987	0.0788	0.0138	0.0078	0.0014	400
52	1.2545	-0.2502	0.0341	-0.0691	0.0742	0.0123	0.0073	0.0012	400
53	1.2545	-0.0001	0.0542	-0.0255	0.1133	0.0215	0.0079	0.0015	800
54	1.2545	0.2498	0.0600	-0.0090	0.1021	0.0183	0.0076	0.0014	700
55	1.2545	0.5001	0.0638	-0.0031	0.1034	0.0178	0.0077	0.0013	700
56	1.5032	-1.0002	-0.0077	-0.0275	0.0719	0.0119	0.0082	0.0013	300
57	1.5032	-0.7497	-0.0135	-0.0329	0.0793	0.0137	0.0078	0.0014	400
58	1.5032	-0.4997	-0.0042	-0.0483	0.0759	0.0122	0.0075	0.0012	400
59	1.5032	-0.2497	0.0314	-0.0409	0.0612	0.0099	0.0070	0.0011	300
60	1.5032	0.0003	0.0433	-0.0229	0.0744	0.0127	0.0073	0.0013	400
61	1.5032	0.2503	0.0620	-0.0098	0.0598	0.0105	0.0068	0.0012	300
62	1.5032	0.5003	0.0508	-0.0013	0.0763	0.0129	0.0075	0.0013	400
63	1.7526	-1.0003	-0.0018	-0.0262	0.0692	0.0114	0.0068	0.0011	400
64	1.7526	-0.7501	0.0002	-0.0292	0.0738	0.0112	0.0073	0.0011	400
65	1.7526	-0.5002	0.0081	-0.0301	0.0730	0.0114	0.0072	0.0011	400
66	1.7526	-0.2502	0.0184	-0.0281	0.0718	0.0121	0.0071	0.0012	400
67	1.7526	-0.0002	0.0342	-0.0143	0.0678	0.0111	0.0078	0.0013	300
68	1.7526	0.2498	0.0499	-0.0057	0.0675	0.0118	0.0067	0.0012	400
69	1.7526	0.5001	0.0563	-0.0033	0.0702	0.0105	0.0080	0.0012	300
70	1.9985	-1.0002	0.0036	-0.0213	0.0661	0.0110	0.0076	0.0012	300
71	2.0003	-0.7497	0.0142	-0.0261	0.0789	0.0126	0.0078	0.0012	400
72	2.0003	-0.4997	0.0082	-0.0193	0.0740	0.0117	0.0084	0.0013	300
73	2.0003	-0.2497	0.0095	-0.0106	0.0912	0.0133	0.0074	0.0011	600
74	2.0003	0.0003	0.0309	-0.0054	0.0865	0.0120	0.0085	0.0012	400
75	2.0003	0.2503	0.0452	0.0002	0.0755	0.0127	0.0075	0.0013	400
76	2.0003	0.5003	0.0333	0.0031	0.0800	0.0113	0.0079	0.0011	400
77	2.2493	-1.0003	0.0146	-0.0208	0.0884	0.0131	0.0078	0.0012	500
78	2.2493	-0.7501	0.0182	-0.0210	0.0913	0.0131	0.0074	0.0011	600
79	2.2493	-0.5002	0.0010	-0.0101	0.0834	0.0127	0.0082	0.0013	400
80	2.2493	-0.2502	0.0061	-0.0032	0.0946	0.0133	0.0083	0.0012	500
81	2.2493	-0.0001	0.0175	0.0031	0.0939	0.0136	0.0075	0.0011	600
82	2.2493	0.2498	0.0199	0.0083	0.0837	0.0128	0.0083	0.0013	400
83	2.2493	0.5001	0.0194	0.0103	0.0923	0.0141	0.0081	0.0012	500
84	2.4969	-1.0002	-0.0101	-0.0154	0.0884	0.0132	0.0087	0.0013	400
85	2.4969	-0.7497	0.0146	-0.0152	0.0921	0.0134	0.0081	0.0012	500
86	2.4969	-0.4997	0.0171	-0.0110	0.0824	0.0117	0.0073	0.0010	500
87	2.4969	-0.2497	0.0189	-0.0011	0.0888	0.0125	0.0078	0.0011	500
88	2.4969	0.0003	0.0329	0.0027	0.0916	0.0130	0.0081	0.0012	500
89	2.4969	0.2503	0.0323	0.0079	0.1005	0.0144	0.0081	0.0012	600
90	2.4969	0.5003	0.0105	0.0078	0.1246	0.0136	0.0093	0.0010	700

TABLE 5. - SMALL VELOCITY GRID DATA, CONFIGURATION NUMBER 2

	y/c	z/c	v	w	σ_v	σ_w	Tol_v	Tol_w	N
1	0.7528	-0.7498	-0.0196	0.0569	0.0581	0.0115	0.0081	0.0016	200
2	0.7528	-0.6873	-0.0312	0.0783	0.0509	0.0097	0.0071	0.0013	200
3	0.7528	-0.6247	-0.0141	0.0906	0.0502	0.0103	0.0070	0.0014	200
4	0.7528	-0.5623	0.0008	0.1035	0.0649	0.0131	0.0074	0.0015	300
5	0.7528	-0.4997	0.0151	0.1073	0.0713	0.0138	0.0081	0.0016	300
6	0.7528	-0.4373	0.0501	0.1006	0.0743	0.0146	0.0084	0.0017	300
7	0.7528	-0.3748	0.0471	0.0978	0.0841	0.0167	0.0074	0.0015	500
8	0.7528	-0.3123	0.0398	0.0925	0.0699	0.0127	0.0069	0.0013	400
9	0.7528	-0.2498	0.0498	0.0875	0.0691	0.0133	0.0079	0.0015	300
10	0.8166	-0.7501	-0.0365	0.0586	0.0472	0.0082	0.0066	0.0011	200
11	0.8166	-0.6876	-0.0537	0.0834	0.0468	0.0090	0.0065	0.0013	200
12	0.8166	-0.6252	-0.0277	0.1024	0.0492	0.0098	0.0069	0.0014	200
13	0.8166	-0.5626	0.0040	0.1215	0.0591	0.0122	0.0067	0.0014	300
14	0.8166	-0.5001	0.0167	0.1314	0.0742	0.0151	0.0073	0.0015	400
15	0.8166	-0.4376	0.0619	0.1190	0.0858	0.0163	0.0075	0.0014	500
16	0.8166	-0.3751	0.0525	0.1087	0.0876	0.0167	0.0077	0.0015	500
17	0.8166	-0.3126	0.0638	0.0932	0.0753	0.0145	0.0086	0.0017	300
18	0.8166	-0.2498	0.0605	0.0843	0.0968	0.0187	0.0085	0.0017	500
19	0.8779	-0.7501	-0.0887	0.0593	0.0508	0.0084	0.0071	0.0012	200
20	0.8779	-0.6873	-0.0759	0.0835	0.0483	0.0094	0.0067	0.0013	200
21	0.8779	-0.6247	-0.0697	0.1194	0.0542	0.0100	0.0076	0.0014	200
22	0.8779	-0.5623	-0.0184	0.1555	0.0912	0.0182	0.0081	0.0016	500
23	0.8779	-0.4997	0.0503	0.1716	0.1429	0.0254	0.0078	0.0014	1300
24	0.8779	-0.4373	0.0897	0.1476	0.1302	0.0227	0.0081	0.0014	1000
25	0.8779	-0.3748	0.0804	0.1165	0.1076	0.0193	0.0075	0.0013	800
26	0.8779	-0.3123	0.0619	0.0980	0.0892	0.0164	0.0072	0.0013	600
27	0.8779	-0.2498	0.0644	0.0820	0.0907	0.0170	0.0073	0.0014	600
28	0.9415	-0.7498	-0.0860	0.0434	0.0623	0.0089	0.0061	0.0009	400
29	0.9415	-0.6873	-0.1043	0.0694	0.0512	0.0075	0.0071	0.0010	200
30	0.9415	-0.6247	-0.1587	0.1211	0.1098	0.0153	0.0077	0.0011	800
31	0.9415	-0.5623	-0.1149	0.2127	0.1749	0.0290	0.0081	0.0013	1800
32	0.9415	-0.4998	0.0519	0.2477	0.1905	0.0350	0.0084	0.0015	2000
33	0.9415	-0.4373	0.1231	0.1625	0.2089	0.0366	0.0092	0.0016	2000
34	0.9415	-0.3748	0.1012	0.1098	0.1489	0.0275	0.0078	0.0014	1400
35	0.9415	-0.3123	0.0880	0.0856	0.0821	0.0159	0.0066	0.0013	600
36	0.9415	-0.2498	0.0733	0.0803	0.0855	0.0166	0.0069	0.0013	600
37	1.0041	-0.7501	-0.0891	0.0235	0.0701	0.0113	0.0069	0.0011	400
38	1.0041	-0.6876	-0.1181	0.0360	0.0882	0.0129	0.0071	0.0010	600
39	1.0041	-0.6251	-0.1784	0.0552	0.2004	0.0313	0.0088	0.0014	2000
40	1.0041	-0.5626	-0.1809	0.1250	0.3215	0.0520	0.0141	0.0023	2000
41	1.0041	-0.4376	0.2104	0.1020	0.2423	0.0433	0.0107	0.0019	2000
42	1.0041	-0.3751	0.1221	0.0718	0.1219	0.0217	0.0076	0.0014	1000
43	1.0041	-0.3126	0.1039	0.0662	0.0829	0.0151	0.0067	0.0012	600
44	1.0041	-0.2498	0.0916	0.0623	0.0726	0.0139	0.0071	0.0014	400
45	1.0658	-0.7501	-0.0974	-0.0066	0.0913	0.0157	0.0073	0.0013	600
46	1.0658	-0.6873	-0.1489	-0.0120	0.1265	0.0199	0.0079	0.0012	1000
47	1.0658	-0.6247	-0.2008	-0.0448	0.2281	0.0411	0.0100	0.0018	2000
48	1.0658	-0.5623	-0.2690	-0.1250	0.3359	0.0611	0.0147	0.0027	2000
49	1.0658	-0.4997	0.0897	-0.2130	0.3176	0.0529	0.0140	0.0023	2000
50	1.0658	-0.4373	0.1636	-0.0475	0.2195	0.0391	0.0097	0.0017	2000

TABLE 5. - CONCLUDED

	y/c	z/c	v	w	σ_v	σ_w	Tol_v	Tol_w	N
51	1.0658	-0.3748	0.1217	0.0238	0.0999	0.0170	0.0080	0.0014	600
52	1.0658	-0.3123	0.0949	0.0438	0.0833	0.0142	0.0067	0.0011	600
53	1.0658	-0.2498	0.0855	0.0493	0.0572	0.0109	0.0080	0.0015	200
54	1.1297	-0.7501	-0.0899	-0.0283	0.0936	0.0173	0.0075	0.0014	600
55	1.1297	-0.6876	-0.1056	-0.0462	0.1245	0.0231	0.0071	0.0013	1200
56	1.1297	-0.6251	-0.1186	-0.0923	0.1529	0.0284	0.0080	0.0015	1400
57	1.1297	-0.5626	-0.0834	-0.1343	0.1681	0.0321	0.0078	0.0015	1800
58	1.1297	-0.5001	0.0217	-0.1396	0.1499	0.0260	0.0079	0.0014	1400
59	1.1297	-0.4376	0.0668	-0.0575	0.1278	0.0219	0.0080	0.0014	1000
60	1.1297	-0.3751	0.0774	-0.0004	0.0804	0.0124	0.0079	0.0012	400
61	1.1297	-0.3126	0.0668	0.0318	0.0799	0.0121	0.0079	0.0012	400
62	1.1297	-0.2498	0.0649	0.0486	0.0785	0.0143	0.0077	0.0014	400
63	1.1910	-0.7501	-0.0784	-0.0371	0.0864	0.0167	0.0069	0.0013	600
64	1.2545	-0.7498	-0.0595	-0.0449	0.0929	0.0179	0.0075	0.0014	600
65	1.2545	-0.6874	-0.0544	-0.0581	0.0922	0.0171	0.0081	0.0015	500
66	1.1910	-0.6873	-0.0822	-0.0622	0.0962	0.0173	0.0077	0.0014	600
67	1.1910	-0.6247	-0.0880	-0.0822	0.1168	0.0216	0.0073	0.0013	1000
68	1.2545	-0.6247	-0.0631	-0.0709	0.1030	0.0200	0.0077	0.0015	700
69	1.1910	-0.5623	-0.0602	-0.1131	0.1082	0.0204	0.0075	0.0014	800
70	1.2545	-0.5623	-0.0395	-0.0929	0.0965	0.0182	0.0085	0.0016	500
71	1.1910	-0.4998	-0.0364	-0.1225	0.1240	0.0235	0.0077	0.0015	1000
72	1.2545	-0.4997	-0.0216	-0.0970	0.0864	0.0172	0.0085	0.0017	400
73	1.1910	-0.4373	0.0009	-0.0952	0.1938	0.0325	0.0085	0.0014	2000
74	1.2545	-0.4373	-0.0067	-0.0959	0.0740	0.0156	0.0073	0.0015	400
75	1.1910	-0.3748	0.0435	-0.0569	0.2396	0.0383	0.0105	0.0017	2000
76	1.2545	-0.3747	0.0126	-0.0919	0.0750	0.0151	0.0074	0.0015	400
77	1.1910	-0.3123	0.0178	-0.0201	0.2486	0.0395	0.0109	0.0017	2000
78	1.2545	-0.3123	0.0216	-0.0802	0.0824	0.0163	0.0082	0.0016	400
79	1.1910	-0.2498	0.0602	0.0055	0.2386	0.0381	0.0105	0.0017	2000
80	1.2545	-0.2497	0.0128	-0.0622	0.0848	0.0165	0.0084	0.0016	400

TABLE 6. - LARGE VELOCITY GRID DATA, CONFIGURATION NUMBER 3

	y/c	z/c	v	w	σ_v	σ_w	Tol_v	Tol_w	N
1	-0.5033	-0.9999	0.0239	0.0230	0.0476	0.0103	0.0066	0.0015	200
2	-0.5033	-0.7498	0.0303	0.0131	0.0381	0.0078	0.0075	0.0015	100
3	-0.5033	-0.5001	0.0369	0.0311	0.0491	0.0116	0.0068	0.0016	200
4	-0.5033	-0.2497	0.0158	0.0381	0.0528	0.0116	0.0074	0.0016	200
5	-0.5033	0.0002	0.0307	0.0347	0.0404	0.0091	0.0080	0.0018	100
6	-0.5033	0.2503	0.0550	0.0298	0.0532	0.0112	0.0074	0.0016	200
7	-0.5033	0.5003	0.0407	0.0254	0.0380	0.0070	0.0075	0.0014	100
8	-0.2521	-1.0002	0.0200	0.0331	0.0640	0.0141	0.0073	0.0016	300
9	-0.2521	-0.7501	0.0158	0.0275	0.0584	0.0118	0.0081	0.0016	200
10	-0.2521	-0.4997	0.0194	0.0375	0.0415	0.0087	0.0081	0.0017	100
11	-0.2521	-0.2502	0.0239	0.0408	0.0448	0.0093	0.0062	0.0013	200
12	-0.2521	-0.0002	0.0341	0.0419	0.0474	0.0104	0.0066	0.0015	200
13	-0.2521	0.2498	0.0400	0.0495	0.0376	0.0064	0.0074	0.0013	100
14	-0.2521	0.5000	0.0583	0.0337	0.0402	0.0086	0.0079	0.0017	100
15	-0.0010	-1.0001	0.0155	0.0357	0.0522	0.0099	0.0073	0.0014	200
16	-0.0010	-0.7498	0.0021	0.0498	0.0544	0.0115	0.0076	0.0016	200
17	-0.0010	-0.4997	0.0206	0.0485	0.0490	0.0101	0.0068	0.0014	200
18	-0.0010	-0.2497	0.0259	0.0530	0.0502	0.0105	0.0070	0.0015	200
19	-0.0010	0.0002	0.0509	0.0491	0.0672	0.0143	0.0076	0.0016	300
20	-0.0010	0.2503	0.0651	0.0448	0.0688	0.0143	0.0078	0.0016	300
21	-0.0010	0.5003	0.0521	0.0380	0.0525	0.0107	0.0073	0.0015	200
22	0.2501	-1.0003	-0.0013	0.0409	0.0509	0.0098	0.0071	0.0014	200
23	0.2501	-0.7501	0.0026	0.0549	0.0536	0.0111	0.0074	0.0016	200
24	0.2501	-0.5002	0.0317	0.0623	0.0581	0.0117	0.0081	0.0016	200
25	0.2501	-0.2502	0.0505	0.0605	0.0538	0.0106	0.0075	0.0015	200
26	0.2501	-0.0002	0.0433	0.0709	0.0537	0.0111	0.0075	0.0016	200
27	0.2501	0.2499	0.0745	0.0503	0.0629	0.0128	0.0071	0.0015	300
28	0.2501	0.5000	0.0697	0.0479	0.0730	0.0144	0.0083	0.0016	300
29	0.5017	-1.0001	-0.0194	0.0450	0.0737	0.0138	0.0084	0.0016	300
30	0.5017	-0.7498	-0.0124	0.0731	0.0585	0.0120	0.0066	0.0014	300
31	0.5017	-0.4997	0.0220	0.0919	0.0538	0.0110	0.0061	0.0013	300
32	0.5017	-0.2497	0.0598	0.0905	0.0652	0.0136	0.0074	0.0016	300
33	0.5017	0.0002	0.0602	0.0825	0.0636	0.0135	0.0072	0.0015	300
34	0.5017	0.2503	0.0819	0.0630	0.0528	0.0111	0.0073	0.0015	200
35	0.5017	0.5003	0.0611	0.0564	0.0655	0.0134	0.0074	0.0015	300
36	0.7528	-1.0003	-0.0460	0.0386	0.0639	0.0133	0.0073	0.0015	300
37	0.7528	-0.7502	-0.0496	0.0890	0.0600	0.0134	0.0068	0.0015	300
38	0.7528	-0.5001	0.0157	0.1624	0.0712	0.0145	0.0081	0.0017	300
39	0.7528	-0.2502	0.0963	0.1100	0.0845	0.0171	0.0074	0.0015	500
40	0.7528	-0.0001	0.0712	0.0868	0.0878	0.0201	0.0077	0.0018	500
41	0.7528	0.2498	0.0952	0.0652	0.0704	0.0145	0.0080	0.0017	300
42	0.7528	0.5000	0.0843	0.0539	0.0778	0.0164	0.0088	0.0019	300
43	1.0041	-1.0002	-0.0561	0.0030	0.0530	0.0088	0.0074	0.0012	200
44	1.0041	-0.7502	-0.1375	0.0161	0.0951	0.0155	0.0076	0.0012	600
45	1.0041	-0.2502	0.1542	0.0632	0.0861	0.0155	0.0084	0.0015	400
46	1.0041	-0.0002	0.0826	0.0713	0.0888	0.0164	0.0078	0.0015	500
47	1.0041	0.2498	0.1014	0.0694	0.0692	0.0122	0.0079	0.0014	300
48	1.0041	0.4999	0.0728	0.0596	0.0665	0.0116	0.0076	0.0013	300
49	1.2545	-1.0002	-0.0637	-0.0245	0.0714	0.0139	0.0081	0.0016	300
50	1.2545	-0.7501	-0.0797	-0.0779	0.0802	0.0145	0.0079	0.0014	400

TABLE 6. - CONCLUDED

	y/c	z/c	v	w	σ_v	σ_w	Tol_v	Tol_w	N
51	1.2545	-0.5002	-0.0478	-0.1569	0.0970	0.0170	0.0078	0.0014	600
52	1.2545	-0.2502	0.0490	-0.0642	0.2482	0.0422	0.0109	0.0019	2000
53	1.2545	-0.0002	0.0378	0.0050	0.2487	0.0417	0.0109	0.0018	2000
54	1.2545	0.2498	0.0847	0.0108	0.2286	0.0390	0.0100	0.0017	2000
55	1.2545	0.4999	0.0662	0.0104	0.2062	0.0361	0.0091	0.0016	2000
56	1.5032	-1.0001	-0.0319	-0.0415	0.0671	0.0115	0.0076	0.0013	300
57	1.5032	-0.7498	-0.0215	-0.0696	0.0656	0.0118	0.0074	0.0013	300
58	1.5032	-0.4997	-0.0122	-0.0860	0.0593	0.0112	0.0083	0.0016	200
59	1.5032	-0.2498	0.0429	-0.0779	0.0594	0.0108	0.0068	0.0012	300
60	1.5032	0.0002	0.0633	-0.0517	0.0716	0.0142	0.0099	0.0020	200
61	1.5032	0.2501	0.0905	-0.0328	0.0618	0.0103	0.0070	0.0012	300
62	1.5032	0.5003	0.0652	-0.0158	0.0682	0.0133	0.0078	0.0015	300
63	1.7526	-1.0002	-0.0143	-0.0442	0.0672	0.0109	0.0077	0.0012	300
64	1.7526	-0.7501	-0.0077	-0.0475	0.0811	0.0135	0.0080	0.0013	400
65	1.7526	-0.5001	-0.0012	-0.0618	0.0715	0.0116	0.0082	0.0013	300
66	1.7526	-0.2502	0.0247	-0.0536	0.0674	0.0111	0.0077	0.0013	300
67	1.7526	-0.0002	0.0487	-0.0385	0.0719	0.0118	0.0082	0.0013	300
68	1.7526	0.2499	0.0792	-0.0310	0.0670	0.0115	0.0077	0.0013	300
69	1.7526	0.5000	0.0676	-0.0202	0.0701	0.0125	0.0080	0.0014	300
70	2.0003	-1.0001	-0.0065	-0.0334	0.0572	0.0088	0.0081	0.0012	200
71	2.0003	-0.7498	0.0030	-0.0442	0.0717	0.0122	0.0071	0.0012	400
72	2.0003	-0.4997	0.0003	-0.0387	0.0826	0.0127	0.0082	0.0013	400
73	2.0003	-0.2497	0.0219	-0.0361	0.0675	0.0107	0.0077	0.0012	300
74	2.0003	0.0002	0.0252	-0.0255	0.0770	0.0131	0.0076	0.0013	400
75	2.0003	0.2501	0.0378	-0.0171	0.0754	0.0124	0.0075	0.0012	400
76	2.0003	0.5003	0.0426	-0.0096	0.0748	0.0118	0.0086	0.0013	300
77	2.2493	-1.0002	0.0105	-0.0329	0.0813	0.0130	0.0072	0.0012	500
78	2.2493	-0.7501	0.0101	-0.0312	0.0844	0.0135	0.0084	0.0013	400
79	2.2493	-0.5002	0.0183	-0.0313	0.0748	0.0122	0.0074	0.0012	400
80	2.2493	-0.2501	0.0230	-0.0241	0.0832	0.0129	0.0082	0.0013	400
81	2.2493	-0.0001	0.0323	-0.0169	0.0846	0.0133	0.0075	0.0012	500
82	2.2493	0.2499	0.0606	-0.0137	0.0857	0.0119	0.0076	0.0010	500
83	2.2493	0.5000	0.0271	-0.0075	0.0827	0.0120	0.0082	0.0012	400
84	2.4969	-1.0001	0.0076	-0.0298	0.0808	0.0129	0.0080	0.0013	400
85	2.4969	-0.7498	0.0150	-0.0274	0.0850	0.0144	0.0084	0.0014	400
86	2.4969	-0.4997	0.0081	-0.0244	0.0891	0.0145	0.0079	0.0013	500
87	2.4969	-0.2497	0.0330	-0.0162	0.0822	0.0124	0.0081	0.0012	400
88	2.4969	0.0002	0.0314	-0.0123	0.0867	0.0141	0.0077	0.0012	500
89	2.4969	0.2501	0.0242	-0.0040	0.0862	0.0130	0.0076	0.0012	500
90	2.4969	0.5001	0.0272	-0.0048	0.0906	0.0136	0.0080	0.0012	500

TABLE 7. - SMALL VELOCITY GRID DATA, CONFIGURATION NUMBER 3

	y/c	z/c	v	w	σ_v	σ_w	Tol_v	Tol_w	N
1	0.7528	-0.7502	-0.0496	0.0890	0.0600	0.0134	0.0068	0.0015	300
2	0.7528	-0.6877	-0.0586	0.1114	0.0547	0.0125	0.0076	0.0017	200
3	0.7528	-0.6252	-0.0598	0.1391	0.0573	0.0129	0.0080	0.0018	200
4	0.7528	-0.5626	-0.0225	0.1514	0.0760	0.0165	0.0075	0.0016	400
5	0.7528	-0.5001	0.0157	0.1624	0.0712	0.0145	0.0081	0.0017	300
6	0.7528	-0.4378	0.0238	0.1562	0.0896	0.0193	0.0079	0.0017	500
7	0.7528	-0.3752	0.0564	0.1483	0.0754	0.0152	0.0085	0.0017	300
8	0.7528	-0.3128	0.0882	0.1228	0.0796	0.0169	0.0078	0.0017	400
9	0.7528	-0.2502	0.0963	0.1100	0.0845	0.0171	0.0074	0.0015	500
10	0.8166	-0.7501	-0.0811	0.0884	0.0659	0.0150	0.0075	0.0017	300
11	0.8166	-0.6874	-0.0737	0.1169	0.0601	0.0141	0.0084	0.0020	200
12	0.8166	-0.6248	-0.0668	0.1520	0.0684	0.0165	0.0096	0.0023	200
13	0.8166	-0.5623	-0.0333	0.1803	0.0804	0.0188	0.0079	0.0019	400
14	0.8166	-0.4997	0.0159	0.1984	0.0907	0.0194	0.0080	0.0017	500
15	0.8166	-0.4373	0.0336	0.1898	0.1410	0.0311	0.0080	0.0018	1200
16	0.8166	-0.3747	0.0631	0.1563	0.0909	0.0180	0.0080	0.0016	500
17	0.8166	-0.3124	0.0663	0.1380	0.1349	0.0315	0.0080	0.0019	1100
18	0.8166	-0.2497	0.0845	0.1176	0.0960	0.0220	0.0084	0.0020	500
19	0.8779	-0.7501	-0.1090	0.0816	0.0552	0.0107	0.0063	0.0012	300
20	0.8779	-0.6876	-0.1179	0.1145	0.0411	0.0071	0.0081	0.0014	100
21	0.8779	-0.6252	-0.1214	0.1731	0.0802	0.0167	0.0071	0.0015	500
22	0.8779	-0.5626	-0.1064	0.2414	0.1293	0.0251	0.0080	0.0016	1000
23	0.8779	-0.5002	0.0126	0.2721	0.1496	0.0287	0.0078	0.0015	1400
24	0.8779	-0.4376	0.1012	0.2369	0.1538	0.0283	0.0078	0.0014	1500
25	0.8779	-0.3751	0.1336	0.1757	0.1276	0.0242	0.0079	0.0015	1000
26	0.8779	-0.3126	0.1204	0.1361	0.1225	0.0234	0.0076	0.0015	1000
27	0.8779	-0.2500	0.0766	0.1214	0.1173	0.0241	0.0082	0.0017	800
28	0.9415	-0.7499	-0.1361	0.0555	0.0593	0.0090	0.0082	0.0013	200
29	0.9415	-0.6874	-0.1533	0.0884	0.0689	0.0117	0.0078	0.0013	300
30	0.9415	-0.6248	-0.2160	0.1516	0.1427	0.0235	0.0081	0.0013	1200
31	0.9415	-0.5623	-0.2144	0.2755	0.2357	0.0421	0.0104	0.0019	2000
32	0.9415	-0.4998	-0.0730	0.3867	0.2491	0.0476	0.0109	0.0021	2000
33	0.9415	-0.4373	0.1651	0.2762	0.2678	0.0518	0.0118	0.0023	2000
34	0.9415	-0.3747	0.2268	0.1553	0.1794	0.0309	0.0079	0.0014	2000
35	0.9415	-0.3124	0.1541	0.1169	0.1137	0.0199	0.0079	0.0014	800
36	0.9415	-0.2497	0.1464	0.0900	0.0871	0.0155	0.0086	0.0015	400
37	1.0041	-0.7502	-0.1375	0.0161	0.0951	0.0155	0.0076	0.0012	600
38	1.0041	-0.6877	-0.1937	0.0346	0.1065	0.0159	0.0079	0.0012	700
39	1.0041	-0.6251	-0.2857	0.0487	0.2242	0.0359	0.0098	0.0016	2000
40	1.0041	-0.5626	-0.5039	0.1326	0.3449	0.0499	0.0151	0.0022	2000
41	1.0041	-0.4378	0.2906	0.1083	0.3575	0.0625	0.0157	0.0027	2000
42	1.0041	-0.3752	0.2421	0.0780	0.2072	0.0353	0.0091	0.0016	2000
43	1.0041	-0.3128	0.1866	0.0636	0.1002	0.0162	0.0088	0.0014	500
44	1.0041	-0.2502	0.1542	0.0632	0.0861	0.0155	0.0084	0.0015	400
45	1.0658	-0.7501	-0.1204	-0.0111	0.0857	0.0148	0.0085	0.0015	400
46	1.0658	-0.6873	-0.1546	-0.0314	0.1247	0.0200	0.0082	0.0013	900
47	1.0658	-0.6248	-0.2126	-0.0623	0.2520	0.0451	0.0110	0.0020	2000
48	1.0658	-0.5623	-0.1814	-0.1957	0.3714	0.0613	0.0163	0.0027	2000
49	1.0658	-0.4997	-0.0586	-0.3876	0.3309	0.0557	0.0146	0.0024	2000
50	1.0658	-0.4373	0.3902	-0.1411	0.2887	0.0455	0.0127	0.0020	2000

TABLE 7. - CONCLUDED

	y/c	z/c	v	w	σ_v	σ_w	Tol_v	Tol_w	N
51	1.0658	-0.3747	0.2780	-0.0231	0.1394	0.0214	0.0083	0.0013	1100
52	1.0658	-0.3124	0.2067	0.0260	0.0888	0.0144	0.0078	0.0013	500
53	1.0658	-0.2498	0.1617	0.0420	0.0638	0.0097	0.0073	0.0011	300
54	1.1297	-0.7502	-0.1419	-0.0372	0.1069	0.0178	0.0079	0.0013	700
55	1.1297	-0.6877	-0.1576	-0.0719	0.1330	0.0225	0.0079	0.0013	1100
56	1.1297	-0.6252	-0.1685	-0.1175	0.1757	0.0318	0.0079	0.0014	1900
57	1.1297	-0.5626	-0.1281	-0.1897	0.1938	0.0360	0.0085	0.0016	2000
58	1.1297	-0.5001	-0.0054	-0.2328	0.1786	0.0296	0.0080	0.0013	1900
59	1.1297	-0.4376	0.1218	-0.1620	0.1831	0.0320	0.0085	0.0015	1800
60	1.1297	-0.3751	0.1330	-0.0562	0.0881	0.0148	0.0078	0.0013	500
61	1.1297	-0.3126	0.1338	0.0004	0.0609	0.0100	0.0069	0.0011	300
62	1.1297	-0.2500	0.1226	0.0277	0.0596	0.0101	0.0068	0.0012	300
63	1.1910	-0.7501	-0.1207	-0.0586	0.1094	0.0194	0.0076	0.0014	800
64	1.1910	-0.6874	-0.1181	-0.0837	0.0959	0.0164	0.0084	0.0015	500
65	1.1910	-0.6248	-0.1282	-0.1235	0.1181	0.0193	0.0088	0.0014	700
66	1.1910	-0.5623	-0.0986	-0.1643	0.1349	0.0253	0.0080	0.0015	1100
67	1.1910	-0.4998	-0.0168	-0.1592	0.1495	0.0253	0.0082	0.0014	1300
68	1.1910	-0.4373	0.0354	-0.1099	0.1417	0.0204	0.0088	0.0013	1000
69	1.1910	-0.3747	0.0826	-0.0572	0.1141	0.0188	0.0085	0.0014	700
70	1.1910	-0.3124	0.0917	-0.0125	0.1005	0.0157	0.0081	0.0013	600
71	1.1910	-0.2497	0.0973	0.0191	0.0969	0.0153	0.0086	0.0014	500
72	1.2545	-0.7501	-0.0797	-0.0779	0.0802	0.0145	0.0079	0.0014	400
73	1.2545	-0.6876	-0.0829	-0.0931	0.0939	0.0176	0.0082	0.0016	500
74	1.2545	-0.6252	-0.0775	-0.1184	0.0925	0.0171	0.0081	0.0015	500
75	1.2545	-0.5626	-0.0535	-0.1427	0.0973	0.0178	0.0078	0.0014	600
76	1.2545	-0.5002	-0.0478	-0.1569	0.0970	0.0170	0.0078	0.0014	600
77	1.2545	-0.4376	-0.0020	-0.1491	0.1220	0.0214	0.0080	0.0014	900
78	1.2545	-0.3752	0.0179	-0.1227	0.1891	0.0333	0.0083	0.0015	2000
79	1.2545	-0.3128	0.0319	-0.0903	0.2215	0.0372	0.0097	0.0016	2000
80	1.2545	-0.2502	0.0490	-0.0642	0.2482	0.0422	0.0109	0.0019	2000

TABLE 8. - LARGE VELOCITY GRID DATA, CONFIGURATION NUMBER 4

	y/c	z/c	v	w	σ_v	σ_w	Tol_v	Tol_w	N
1	-0.5033	-0.9999	0.0012	0.0264	0.0601	0.0119	0.0083	0.0017	200
2	-0.5033	-0.7498	0.0410	0.0097	0.0377	0.0076	0.0074	0.0015	100
3	-0.5033	-0.4997	0.0286	0.0127	0.0301	0.0065	0.0059	0.0013	100
4	-0.5033	-0.2497	0.0256	0.0238	0.0592	0.0125	0.0067	0.0014	300
5	-0.5033	0.0003	0.0294	0.0315	0.0479	0.0102	0.0067	0.0014	200
6	-0.5033	0.2503	0.0432	0.0273	0.0491	0.0104	0.0068	0.0015	200
7	-0.5033	0.5003	0.0540	0.0230	0.0555	0.0127	0.0078	0.0018	200
8	-0.2521	-1.0002	0.0064	0.0209	0.0480	0.0094	0.0067	0.0013	200
9	-0.2521	-0.7502	0.0222	0.0298	0.0406	0.0080	0.0080	0.0016	100
10	-0.2521	-0.5002	0.0180	0.0320	0.0522	0.0111	0.0073	0.0016	200
11	-0.2521	-0.2502	0.0223	0.0266	0.0529	0.0110	0.0073	0.0015	200
12	-0.2521	-0.0002	0.0133	0.0421	0.0630	0.0136	0.0087	0.0019	200
13	-0.2521	0.2498	0.0227	0.0342	0.0605	0.0126	0.0069	0.0014	300
14	-0.2521	0.5001	0.0355	0.0367	0.0510	0.0103	0.0071	0.0014	200
15	-0.0010	-1.0001	0.0021	0.0250	0.0552	0.0107	0.0076	0.0015	200
16	-0.0010	-0.7498	0.0235	0.0289	0.0584	0.0113	0.0066	0.0013	300
17	-0.0010	-0.4997	0.0127	0.0406	0.0535	0.0107	0.0074	0.0015	200
18	-0.0010	-0.2497	0.0353	0.0370	0.0503	0.0098	0.0070	0.0014	200
19	-0.0010	0.0003	0.0393	0.0437	0.0537	0.0104	0.0074	0.0015	200
20	-0.0010	0.2503	0.0506	0.0457	0.0540	0.0115	0.0075	0.0016	200
21	-0.0010	0.5003	0.0580	0.0347	0.0645	0.0111	0.0073	0.0013	300
22	0.2501	-1.0002	0.0162	0.0205	0.0685	0.0130	0.0078	0.0015	300
23	0.2501	-0.7502	0.0102	0.0339	0.0526	0.0108	0.0073	0.0015	200
24	0.2501	-0.5002	0.0207	0.0458	0.0465	0.0090	0.0064	0.0013	200
25	0.2501	-0.2502	0.0298	0.0532	0.0550	0.0116	0.0062	0.0013	300
26	0.2501	-0.0002	0.0206	0.0618	0.0638	0.0131	0.0072	0.0015	300
27	0.2501	0.2498	0.0580	0.0530	0.0530	0.0100	0.0074	0.0014	200
28	0.2501	0.5001	0.0646	0.0443	0.0573	0.0119	0.0065	0.0014	300
29	0.5017	-1.0001	-0.0047	0.0191	0.0595	0.0111	0.0067	0.0013	300
30	0.5017	-0.7498	0.0048	0.0318	0.0549	0.0112	0.0076	0.0016	200
31	0.5017	-0.4997	0.0078	0.0544	0.0496	0.0094	0.0069	0.0013	200
32	0.5017	-0.2497	0.0307	0.0730	0.0601	0.0111	0.0068	0.0013	300
33	0.5017	0.0003	0.0427	0.0760	0.0588	0.0109	0.0067	0.0012	300
34	0.5017	0.2503	0.0621	0.0599	0.0635	0.0117	0.0072	0.0013	300
35	0.5017	0.5003	0.0570	0.0560	0.0492	0.0092	0.0068	0.0013	200
36	0.7528	-1.0002	-0.0078	0.0167	0.0573	0.0109	0.0065	0.0013	300
37	0.7528	-0.7502	-0.0261	0.0315	0.0575	0.0109	0.0065	0.0012	300
38	0.7528	-0.5002	-0.0235	0.0682	0.0513	0.0097	0.0071	0.0014	200
39	0.7528	-0.2502	0.0191	0.1195	0.0619	0.0116	0.0070	0.0013	300
40	0.7528	-0.0002	0.0788	0.0886	0.0700	0.0134	0.0079	0.0015	300
41	0.7528	0.2498	0.0820	0.0679	0.0678	0.0126	0.0077	0.0014	300
42	0.7528	0.5001	0.0719	0.0540	0.0598	0.0119	0.0068	0.0014	300
43	1.0041	-1.0001	0.0049	-0.0000	0.0637	0.0113	0.0072	0.0013	300
44	1.0041	-0.7498	-0.0249	0.0084	0.0627	0.0096	0.0071	0.0011	300
45	1.0041	-0.4997	-0.0767	0.0247	0.0694	0.0113	0.0079	0.0013	300
46	1.0041	0.0003	0.1143	0.0714	0.0795	0.0137	0.0078	0.0014	400
47	1.0041	0.2503	0.0922	0.0622	0.0671	0.0128	0.0076	0.0015	300
48	1.0041	0.5003	0.0989	0.0500	0.0701	0.0133	0.0069	0.0013	400
49	1.2545	-1.0002	0.0038	-0.0082	0.0645	0.0112	0.0073	0.0013	300
50	1.2545	-0.7502	-0.0261	-0.0143	0.0503	0.0095	0.0070	0.0013	200

TABLE 8. - CONCLUDED

	y/c	z/c	v	w	σ_v	σ_w	Tol_v	Tol_w	N
51	1.2545	-0.5002	-0.0512	-0.0358	0.0732	0.0131	0.0072	0.0013	400
52	1.2545	-0.2502	-0.0063	-0.0971	0.0761	0.0136	0.0075	0.0013	400
53	1.2545	-0.0002	0.0548	-0.0638	0.0772	0.0154	0.0076	0.0015	400
54	1.2545	0.2498	0.0809	-0.0340	0.1153	0.0211	0.0081	0.0015	800
55	1.2545	0.5001	0.0660	-0.0142	0.1004	0.0178	0.0081	0.0014	600
56	1.5032	-1.0002	-0.0053	-0.0187	0.0645	0.0119	0.0073	0.0014	300
57	1.5032	-0.7498	-0.0112	-0.0248	0.0731	0.0126	0.0072	0.0013	400
58	1.5032	-0.4997	-0.0241	-0.0331	0.0776	0.0140	0.0076	0.0014	400
59	1.5032	-0.2497	0.0210	-0.0482	0.0694	0.0127	0.0079	0.0015	300
60	1.5032	0.0003	0.0429	-0.0383	0.0591	0.0107	0.0067	0.0012	300
61	1.5032	0.2503	0.0650	-0.0264	0.0504	0.0099	0.0070	0.0014	200
62	1.5032	0.5003	0.0766	-0.0190	0.0579	0.0100	0.0066	0.0011	300
63	1.7526	-1.0002	0.0070	-0.0206	0.0708	0.0114	0.0081	0.0013	300
64	1.7526	-0.7502	0.0063	-0.0242	0.0781	0.0133	0.0077	0.0013	400
65	1.7526	-0.5002	0.0008	-0.0267	0.0816	0.0143	0.0072	0.0013	500
66	1.7526	-0.2501	-0.0013	-0.0245	0.0714	0.0126	0.0082	0.0014	300
67	1.7526	-0.0002	0.0340	-0.0176	0.0761	0.0135	0.0075	0.0013	400
68	1.7526	0.2498	0.0500	-0.0182	0.0704	0.0121	0.0080	0.0014	300
69	1.7526	0.5001	0.0565	-0.0094	0.0834	0.0132	0.0083	0.0013	400
70	2.0003	-1.0001	0.0207	-0.0216	0.0739	0.0125	0.0084	0.0014	300
71	2.0003	-0.7498	0.0145	-0.0193	0.0804	0.0135	0.0079	0.0013	400
72	2.0003	-0.4997	0.0085	-0.0190	0.0784	0.0125	0.0078	0.0012	400
73	2.0003	-0.2497	0.0181	-0.0185	0.0563	0.0094	0.0079	0.0013	200
74	2.0003	0.0003	0.0245	-0.0111	0.0700	0.0114	0.0080	0.0013	300
75	2.0003	0.2503	0.0449	-0.0093	0.0639	0.0100	0.0073	0.0011	300
76	2.0003	0.5001	0.0492	-0.0077	0.0674	0.0110	0.0077	0.0013	300
77	2.2493	-1.0002	0.0152	-0.0165	0.0805	0.0136	0.0080	0.0013	400
78	2.2493	-0.7502	0.0265	-0.0192	0.0705	0.0118	0.0080	0.0013	300
79	2.2493	-0.5002	0.0131	-0.0145	0.0818	0.0132	0.0081	0.0013	400
80	2.2493	-0.2501	0.0232	-0.0113	0.0746	0.0120	0.0074	0.0012	400
81	2.2493	-0.0002	0.0350	-0.0040	0.0684	0.0108	0.0078	0.0012	300
82	2.2493	0.2498	0.0524	-0.0069	0.0792	0.0128	0.0078	0.0013	400
83	2.2493	0.5001	0.0542	-0.0052	0.0793	0.0131	0.0078	0.0013	400
84	2.4969	-1.0001	0.0189	-0.0168	0.0857	0.0142	0.0076	0.0013	500
85	2.4969	-0.7498	0.0369	-0.0202	0.0704	0.0104	0.0080	0.0012	300
86	2.4969	-0.4997	0.0166	-0.0092	0.0857	0.0131	0.0076	0.0012	500
87	2.4969	-0.2497	0.0251	-0.0070	0.0891	0.0146	0.0078	0.0013	500
88	2.4969	0.0003	0.0366	0.0009	0.0823	0.0134	0.0081	0.0013	400
89	2.4969	0.2503	0.0340	0.0060	0.0794	0.0125	0.0070	0.0011	500
90	2.4969	0.5003	0.0570	-0.0037	0.0827	0.0125	0.0073	0.0011	500

TABLE 9. - LARGE VELOCITY GRID DATA, CONFIGURATION NUMBER 5

	y/c	z/c	v	w	σ_v	σ_w	Tol_v	Tol_w	N
1	-0.5033	-0.9999	0.0283	0.0172	0.0532	0.0118	0.0074	0.0017	200
2	-0.5033	-0.7498	0.0205	0.0194	0.0514	0.0106	0.0072	0.0015	200
3	-0.5033	-0.4997	0.0251	0.0193	0.0610	0.0128	0.0069	0.0015	300
4	-0.5033	-0.2497	0.0280	0.0206	0.0509	0.0101	0.0071	0.0014	200
5	-0.5033	0.0003	0.0352	0.0160	0.0597	0.0135	0.0083	0.0019	200
6	-0.5033	0.2503	0.0480	0.0148	0.0488	0.0100	0.0068	0.0014	200
7	-0.5033	0.5003	0.0513	0.0124	0.0534	0.0115	0.0074	0.0016	200
8	-0.2521	-1.0002	0.0342	0.0183	0.0566	0.0110	0.0079	0.0015	200
9	-0.2521	-0.7502	0.0288	0.0207	0.0526	0.0105	0.0073	0.0015	200
10	-0.2521	-0.5002	0.0302	0.0236	0.0580	0.0118	0.0080	0.0016	200
11	-0.2521	-0.2502	0.0163	0.0290	0.0570	0.0107	0.0079	0.0015	200
12	-0.2521	-0.0002	0.0299	0.0268	0.0547	0.0116	0.0076	0.0016	200
13	-0.2521	0.2498	0.0611	0.0241	0.0543	0.0111	0.0075	0.0016	200
14	-0.2521	0.5001	0.0598	0.0167	0.0482	0.0098	0.0067	0.0014	200
15	-0.0010	-1.0002	0.0262	0.0201	0.0512	0.0104	0.0071	0.0015	200
16	-0.0010	-0.7498	0.0333	0.0263	0.0504	0.0095	0.0070	0.0013	200
17	-0.0010	-0.4997	0.0203	0.0328	0.0550	0.0104	0.0076	0.0015	200
18	-0.0010	-0.2497	0.0321	0.0362	0.0544	0.0112	0.0076	0.0016	200
19	-0.0010	0.0003	0.0358	0.0349	0.0528	0.0111	0.0073	0.0016	200
20	-0.0010	0.2503	0.0728	0.0272	0.0572	0.0116	0.0079	0.0016	200
21	-0.0010	0.5003	0.0542	0.0261	0.0596	0.0117	0.0068	0.0013	300
22	0.2501	-1.0002	0.0182	0.0249	0.0557	0.0105	0.0063	0.0012	300
23	0.2501	-0.7502	0.0244	0.0386	0.0494	0.0096	0.0068	0.0013	200
24	0.2501	-0.5002	0.0174	0.0423	0.0537	0.0102	0.0075	0.0014	200
25	0.2501	-0.2502	0.0397	0.0433	0.0511	0.0092	0.0071	0.0013	200
26	0.2501	-0.0002	0.0419	0.0388	0.0635	0.0123	0.0072	0.0014	300
27	0.2501	0.2498	0.0574	0.0357	0.0658	0.0120	0.0075	0.0014	300
28	0.2501	0.5001	0.0706	0.0283	0.0520	0.0106	0.0072	0.0015	200
29	0.5017	-1.0002	0.0072	0.0296	0.0499	0.0092	0.0069	0.0013	200
30	0.5017	-0.7498	0.0106	0.0480	0.0643	0.0118	0.0073	0.0014	300
31	0.5017	-0.4997	0.0180	0.0618	0.0551	0.0098	0.0077	0.0014	200
32	0.5017	-0.2497	0.0458	0.0532	0.0571	0.0106	0.0079	0.0015	200
33	0.5017	0.0003	0.0422	0.0487	0.0562	0.0111	0.0078	0.0016	200
34	0.5017	0.2503	0.0671	0.0434	0.0648	0.0127	0.0073	0.0015	300
35	0.5017	0.5003	0.0654	0.0310	0.0650	0.0126	0.0074	0.0014	300
36	0.7528	-1.0002	-0.0103	0.0208	0.0561	0.0100	0.0078	0.0014	200
37	0.7528	-0.7502	-0.0233	0.0585	0.0531	0.0099	0.0074	0.0014	200
38	0.7528	-0.5002	0.0287	0.0987	0.0703	0.0130	0.0080	0.0015	300
39	0.7528	-0.2502	0.0680	0.0707	0.0561	0.0099	0.0078	0.0014	200
40	0.7528	-0.0002	0.0669	0.0505	0.0585	0.0108	0.0067	0.0012	300
41	0.7528	0.2498	0.0748	0.0466	0.0687	0.0116	0.0078	0.0013	300
42	0.7528	0.5001	0.0783	0.0345	0.0624	0.0112	0.0071	0.0013	300
43	1.0041	-1.0002	-0.0249	0.0008	0.0670	0.0120	0.0076	0.0014	300
44	1.0041	-0.7498	-0.0735	0.0065	0.0803	0.0124	0.0079	0.0012	400
45	1.0041	-0.2497	0.1004	0.0517	0.0769	0.0131	0.0076	0.0013	400
46	1.0041	0.0003	0.0678	0.0533	0.0822	0.0142	0.0081	0.0014	400
47	1.0041	0.2503	0.0768	0.0411	0.0586	0.0111	0.0067	0.0013	300
48	1.0041	0.5003	0.0714	0.0377	0.0748	0.0133	0.0073	0.0013	400
49	1.2545	-1.0002	-0.0263	-0.0215	0.0630	0.0110	0.0071	0.0013	300
50	1.2545	-0.7502	-0.0445	-0.0573	0.0821	0.0144	0.0072	0.0013	500

TABLE 9. - CONCLUDED

	y/c	z/c	v	w	σ_v	σ_w	Tol_v	Tol_w	N
51	1.2545	-0.5002	-0.0089	-0.1188	0.0804	0.0152	0.0079	0.0015	400
52	1.2545	-0.2502	0.0546	-0.0845	0.0962	0.0183	0.0078	0.0015	600
53	1.2545	-0.0002	0.0563	-0.0453	0.1076	0.0215	0.0080	0.0016	700
54	1.2545	0.2498	0.0823	-0.0282	0.1102	0.0182	0.0082	0.0014	700
55	1.2545	0.5001	0.0639	-0.0131	0.1012	0.0166	0.0081	0.0013	600
56	1.5032	-1.0002	-0.0159	-0.0348	0.0784	0.0126	0.0077	0.0012	400
57	1.5032	-0.7498	-0.0174	-0.0515	0.0563	0.0100	0.0079	0.0014	200
58	1.5032	-0.4997	0.0164	-0.0735	0.0660	0.0117	0.0075	0.0013	300
59	1.5032	-0.2497	0.0249	-0.0595	0.0657	0.0108	0.0075	0.0012	300
60	1.5032	0.0003	0.0578	-0.0445	0.0653	0.0116	0.0074	0.0013	300
61	1.5032	0.2503	0.0848	-0.0289	0.0632	0.0105	0.0072	0.0012	300
62	1.5032	0.5003	0.0565	-0.0155	0.0597	0.0098	0.0083	0.0014	200
63	1.7526	-1.0002	0.0022	-0.0350	0.0673	0.0107	0.0077	0.0012	300
64	1.7526	-0.7502	0.0152	-0.0454	0.0709	0.0118	0.0070	0.0012	400
65	1.7526	-0.5002	0.0070	-0.0480	0.0767	0.0134	0.0076	0.0013	400
66	1.7526	-0.2502	0.0252	-0.0449	0.0672	0.0113	0.0076	0.0013	300
67	1.7526	-0.0002	0.0513	-0.0329	0.0647	0.0113	0.0073	0.0013	300
68	1.7526	0.2498	0.0583	-0.0221	0.0716	0.0118	0.0081	0.0014	300
69	1.7526	0.5001	0.0638	-0.0196	0.0713	0.0113	0.0081	0.0013	300
70	2.0003	-1.0002	0.0187	-0.0341	0.0750	0.0131	0.0074	0.0013	400
71	2.0003	-0.7498	0.0155	-0.0390	0.0600	0.0092	0.0084	0.0013	200
72	2.0003	-0.4997	0.0186	-0.0366	0.0683	0.0115	0.0077	0.0013	300
73	2.0003	-0.2497	0.0344	-0.0370	0.0646	0.0111	0.0074	0.0013	300
74	2.0003	0.0003	0.0301	-0.0271	0.0749	0.0132	0.0085	0.0015	300
75	2.0003	0.2503	0.0562	-0.0214	0.0723	0.0114	0.0082	0.0013	300
76	2.0003	0.5003	0.0547	-0.0154	0.0802	0.0138	0.0079	0.0014	400
77	2.2493	-1.0002	0.0209	-0.0303	0.0822	0.0121	0.0081	0.0012	400
78	2.2493	-0.7502	0.0104	-0.0346	0.0932	0.0139	0.0075	0.0011	600
79	2.2493	-0.5002	0.0107	-0.0321	0.0797	0.0129	0.0079	0.0013	400
80	2.2493	-0.2502	0.0302	-0.0258	0.0795	0.0129	0.0079	0.0013	400
81	2.2493	-0.0002	0.0418	-0.0215	0.0923	0.0147	0.0081	0.0013	500
82	2.2493	0.2498	0.0567	-0.0189	0.0714	0.0111	0.0071	0.0011	400
83	2.2493	0.5001	0.0406	-0.0118	0.0676	0.0113	0.0077	0.0013	300
84	2.4969	-1.0002	0.0256	-0.0303	0.0846	0.0115	0.0084	0.0011	400
85	2.4969	-0.7498	0.0269	-0.0257	0.0827	0.0113	0.0082	0.0011	400
86	2.4969	-0.4997	0.0118	-0.0295	0.0872	0.0129	0.0077	0.0011	500
87	2.4969	-0.2497	0.0163	-0.0187	0.0850	0.0125	0.0084	0.0012	400
88	2.4969	0.0003	0.0314	-0.0167	0.0938	0.0148	0.0076	0.0012	600
89	2.4969	0.2503	0.0377	-0.0101	0.0933	0.0146	0.0082	0.0013	500
90	2.4969	0.5003	0.0462	-0.0084	0.0923	0.0145	0.0082	0.0013	500

TABLE 10. - SECTIONAL LIFT COEFFICIENT DISTRIBUTIONS MEASURED BY THE METHOD OF CIRCULATION

Config 2		Config 3		Config 4		Config 5		Config 6	
y/c	c_l	y/c	c_l	y/c	c_l	y/c	c_l	y/c	c_l
2.991	0.519	2.995	0.446	2.993	0.489	2.993	0.191		
2.993	0.515								
2.744	0.505								
2.596	0.509								
2.496	0.481	2.496	0.441	2.496	0.478	2.496	0.188		
2.494	0.476								
2.396	0.500								
2.249	0.504			2.249	0.471	2.249	0.176		
2.249	0.485								
		2.198	0.441						
2.000	0.483	2.000	0.428	2.000	0.466	2.000	0.180	2.000	0.312
2.000	0.489								
1.752	0.468	1.752	0.415	1.752	0.456	1.752	0.176		
		1.603	0.436						
		1.605	0.421						
		1.603	0.426						
1.503	0.472	1.503	0.420	1.503	0.460	1.503	0.185	1.503	0.295
		1.454	0.458						
		1.404	0.468	1.404	0.462	1.404	0.192		
1.354	0.500	1.354	0.437			1.354	0.230		
		1.303	0.412	1.303	0.427	1.303	0.236		
1.254	0.438	1.254	0.470	1.254	0.405	1.254	0.165		
1.204	0.499	1.204	0.510	1.204	0.505	1.204	0.195		
1.154	0.535					1.154	0.261		
1.103	0.535	1.103	0.548	1.103	0.545	1.103	0.272		
1.004	0.541	1.004	0.555	1.004	0.578	1.004	0.288	1.004	0.265
0.903	0.543			0.903	0.592	0.903	0.302		
		0.804	0.583	0.804	0.598	0.804	0.306		
0.752	0.538								
		0.601	0.559	0.601	0.562	0.601	0.302		
				0.601	0.569				
0.501	0.521							0.501	0.223
		0.401	0.526	0.401	0.505	0.401	0.265		
0.250	0.419								
		0.199	0.431	0.199	0.417	0.199	0.220	0.199	0.164
								0.099	0.135
-0.001	0.093	-0.001	0.050	-0.001	0.061	-0.001	0.044		
-0.001	0.063								
-0.051	0.008	-0.051	-0.011						

TABLE 11. - TIP LIFT COEFFICIENT DATA MEASURED BY STRAIN GAGE BALANCE

	Sealed wing/tip junction Configuration					Open wing/tip junction Configuration			
	2	3	4	5	6	2	3	4	5
	.481	.455	.461	.219	.248	.463	.443	.458	.218
	.463	.453	.461	.209	.243	.467	.443	.463	.220
	.474	.456	.459	.218	.235	.470	.445	.446	.213
	.464	.458	.472	.215	.239	.467	.447	.450	.215
	.468	.452	.466	.214	.234	.472	.450	.455	.217
	.478	.453	.462	.217	.237	.467	.449	.452	.221
	.473	.449	.467	.214	.248	.462	.447	.455	.213
	.476	.459	.464	.216	.242	.467	.443	.462	.208
	.474	.459	.464	.205	.242	.466	.447	.456	.219
	.469	.455	.469	.221	.241	.460	.440	.461	.213
	.474	.455	.461	.224	.244	.459	.446	.454	.223
	.466	.447	.473	.225	.245	.473	.444	.457	.219
	.469	.452	.463	.220	.244	.469	.446	.450	.212
	.471	.461	.465	.223	.245	.464	.444	.464	.211
	.471	.459	.462	.225		.464	.443	.460	.219
	.477	.450	.462	.219		.461	.450	.455	.220
	.474	.460	.458	.209		.459	.444	.451	.211
	.479	.456	.462	.219		.471	.442	.459	.216
	.474	.453	.456	.219		.467	.444	.459	.214
	.467	.461	.469	.221		.467	.438	.461	.222
	.460	.451	.462	.224		.468	.438	.461	.224
	.470	.460	.454	.222		.465	.450	.444	.214
	.464	.454	.467	.211		.457	.437	.445	.213
	.465	.462	.465	.216		.459	.453	.464	.207
	.474	.453	.463	.211		.459	.444	.464	
	.478	.465	.475	.216		.465	.442	.449	
	.471	.453		.215		.460	.440		
	.474	.456		.215		.462	.451		
	.462			.227		.469	.441		
	.470			.219		.462	.447		
	.470			.218		.458	.439		
	.470			.217		.466	.443		
				.222					
				.221					
				.212					
				.219					
average	.471	.456	.464	.218	.242	.465	.444	.456	.216
std. dev.	.005	.004	.005	.005	.004	.004	.004	.006	.005
tolerance	.002	.002	.002	.002	.002	.002	.001	.002	.002
corrected	.483	.467	.475	.223	.248	.476	.455	.467	.221
from LV	.471	.470	.481	.228	.250				
disparity	.025	-.006	-.012	-.022	-.008				

TABLE 12. - AVERAGE CALIBRATION DRIFT ERROR[a] FOR VELOCITY GRID DATA

	ϵ_u	ϵ_v	ϵ_w
Configuration 2, large grid	0.0001	0.0195	-0.0043
Configuration 2, small grid	0.0000	0.0155	-0.0032
Configuration 3, large grid	0.0000	0.0179	-0.0038
Configuration 3, small grid	0.0005	0.0185	-0.0044
Configuration 4, large grid	0.0001	0.0195	-0.0042
Configuration 5, large grid	0.0001	0.0195	-0.0042
Configuration 2, large grid [b]	0.0001	0.0194	-0.0042

[a] velocities normalized by u_∞
[b] repeat measurement

TABLE 13. - BLADE TIP DEFLECTIONS

Configuration	Blade deflection (z/c at $y/c = 2.065$)	Tip deflection (z/c at $y/c = 0.00$)
2	0.0010	0.0295
3	0.0213	0.0323
4	0.0119	0.0326
5	-0.0072	0.0145

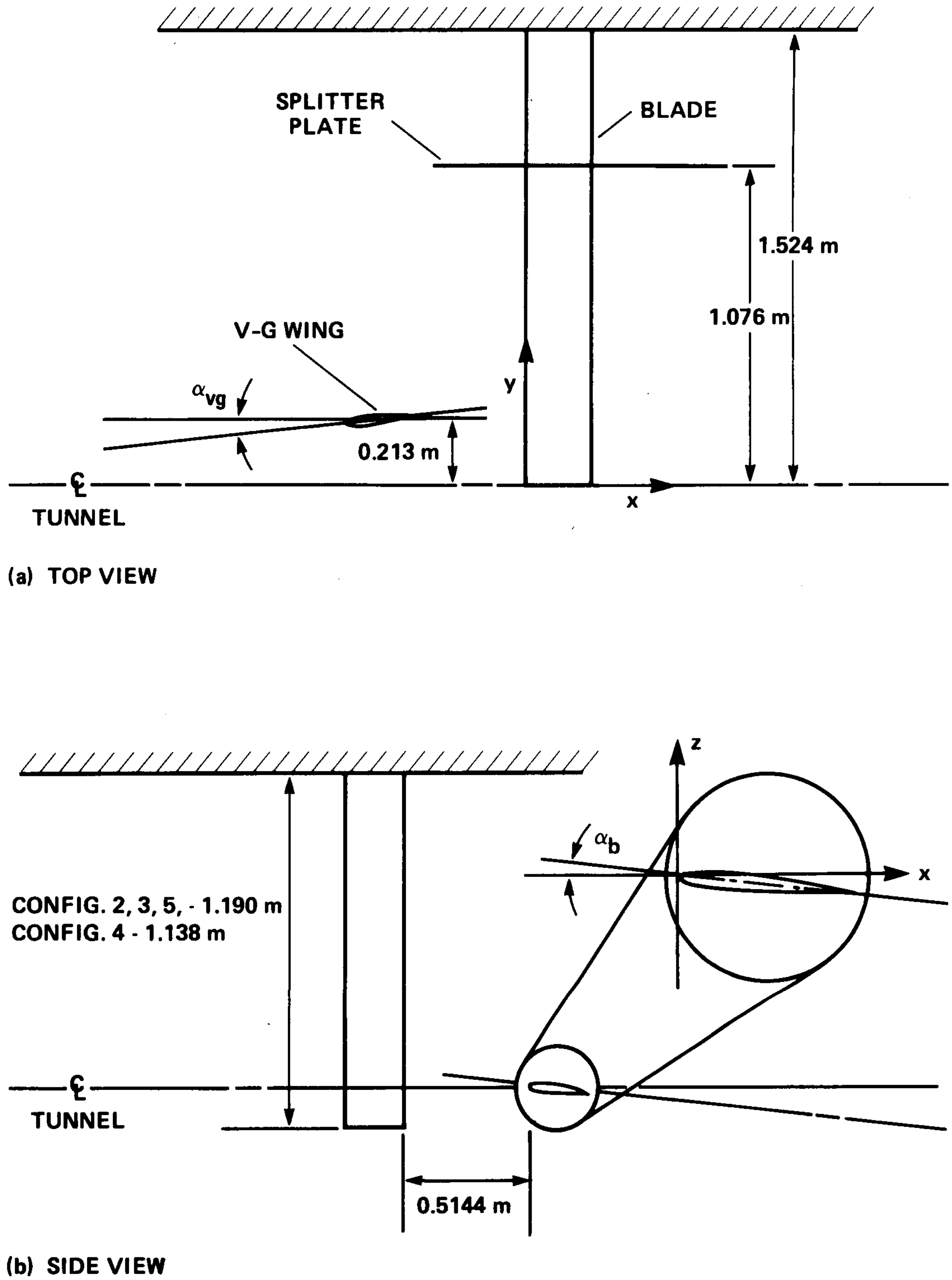

Figure 1. Model geometry.

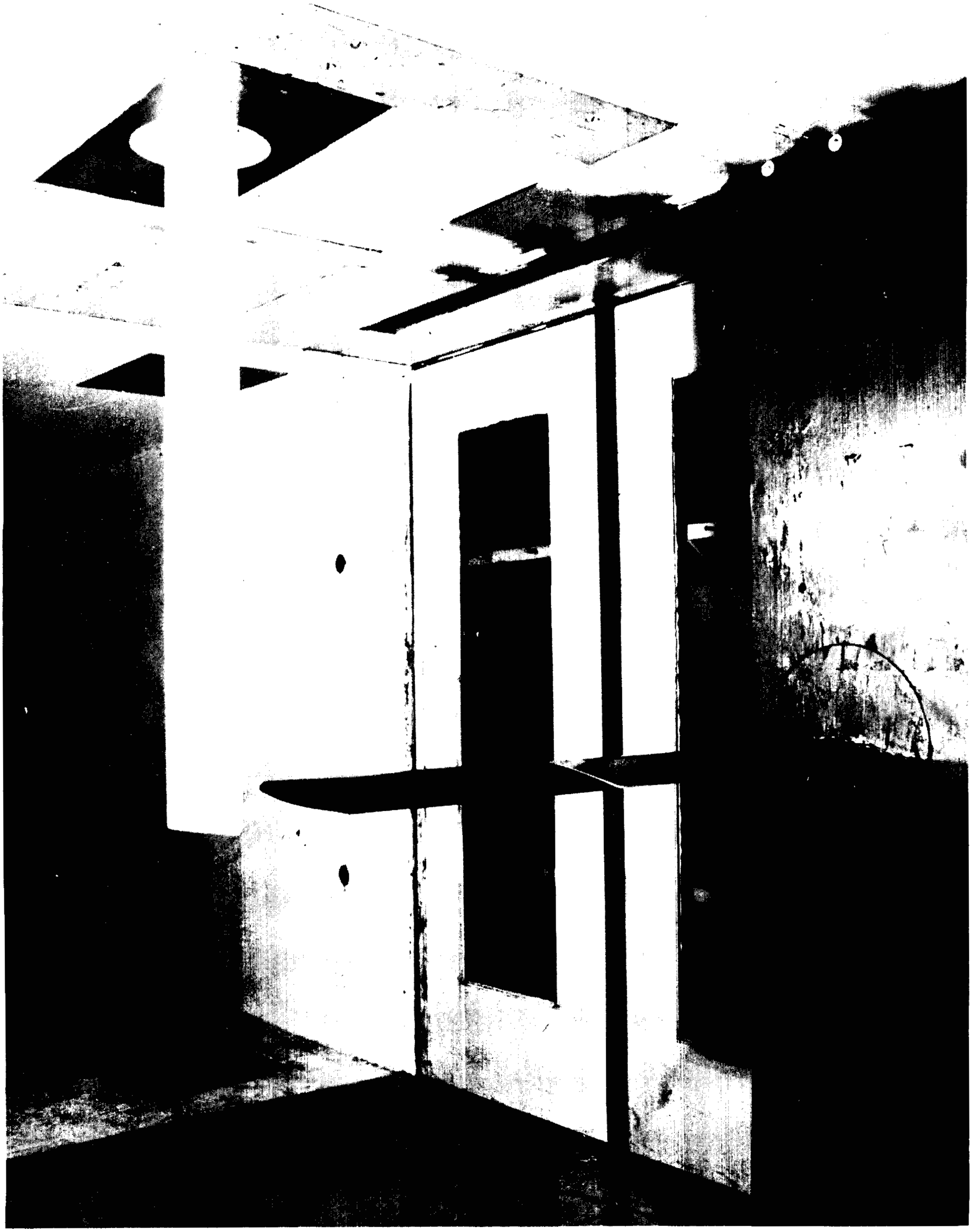

Figure 2. LV measurements of blade-vortex interaction.

ORIGINAL PAGE IS
OF POOR QUALITY

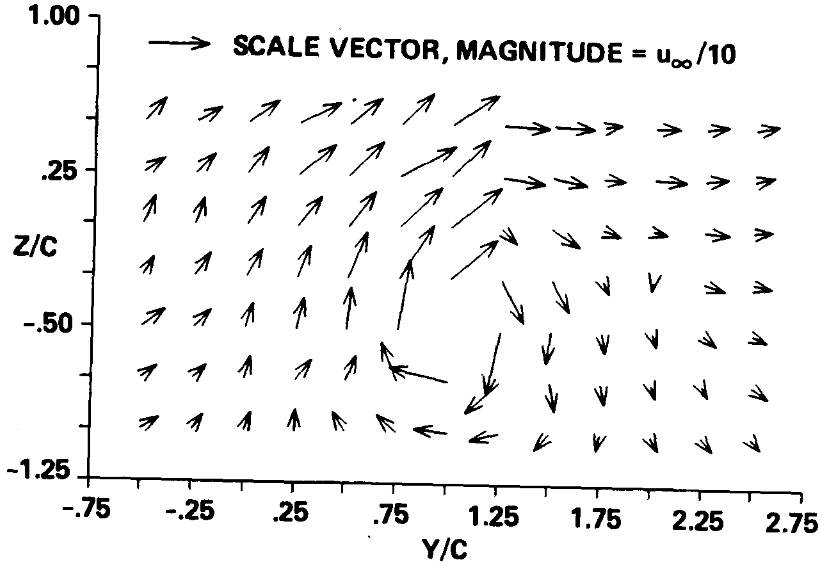

Figure 3. Large velocity grid data, configuration 2.

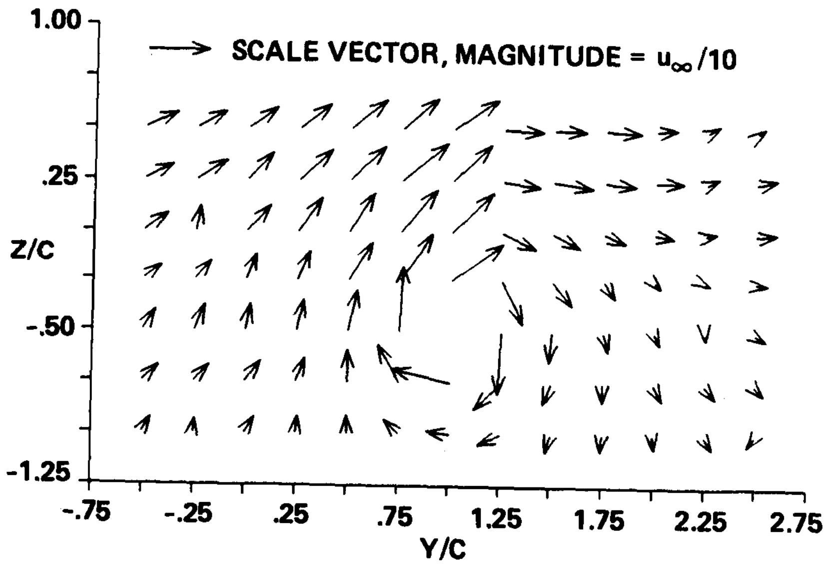

Figure 4. Large velocity grid data, repeat configuration 2.

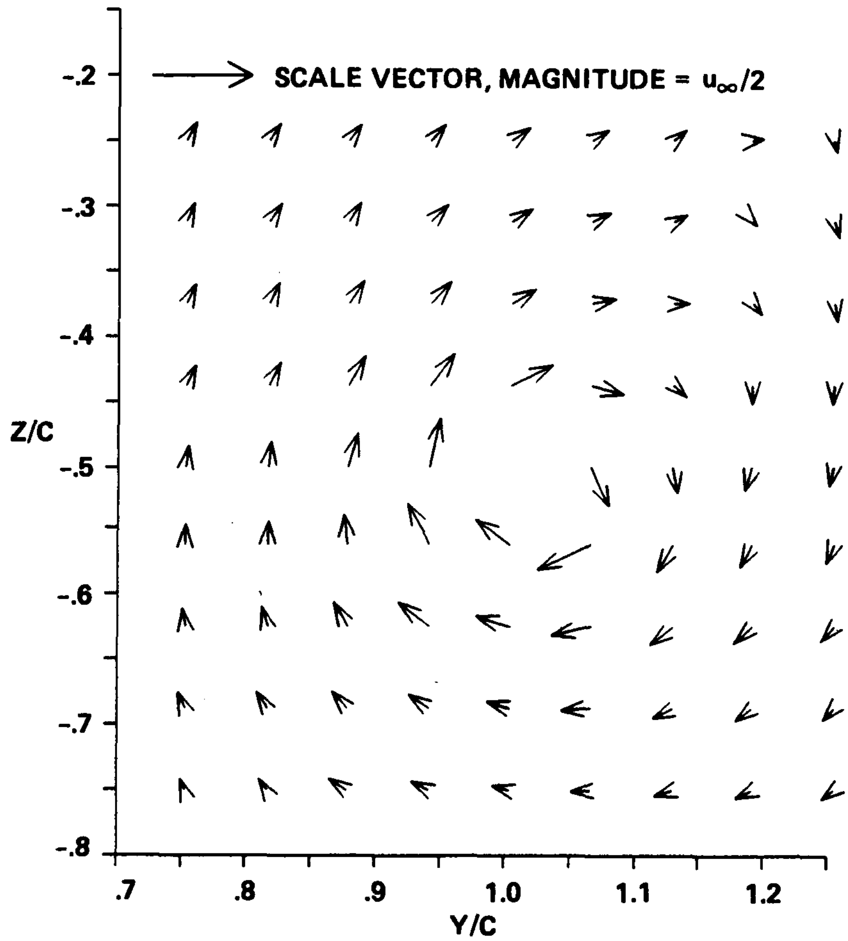

Figure 5. Small velocity grid data, configuration 2.

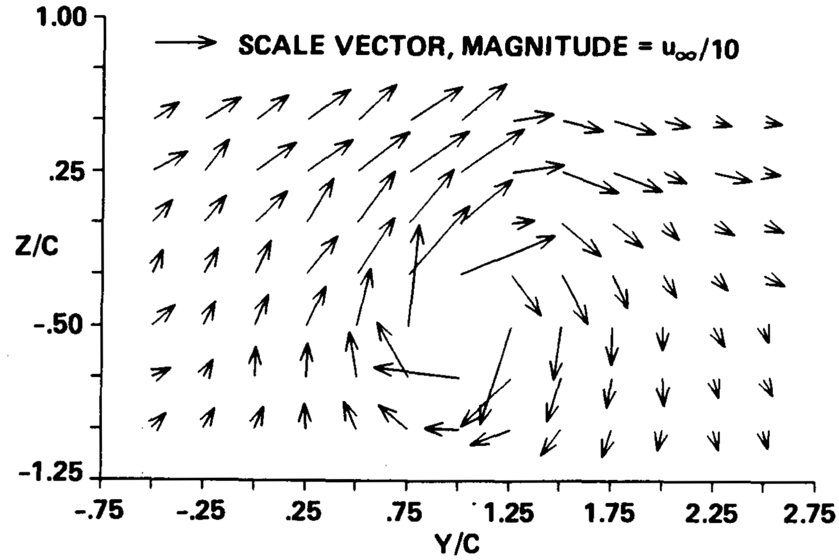

Figure 6. Large velocity grid data, configuration 3.

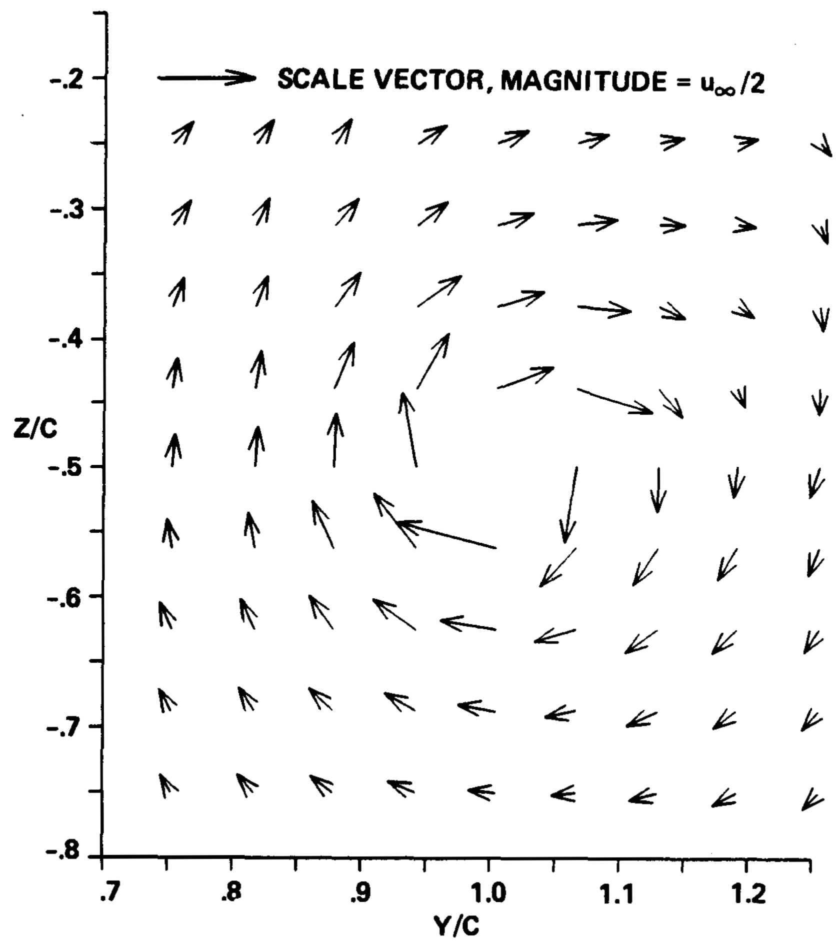

Figure 7. Small velocity grid data, configuration 3.

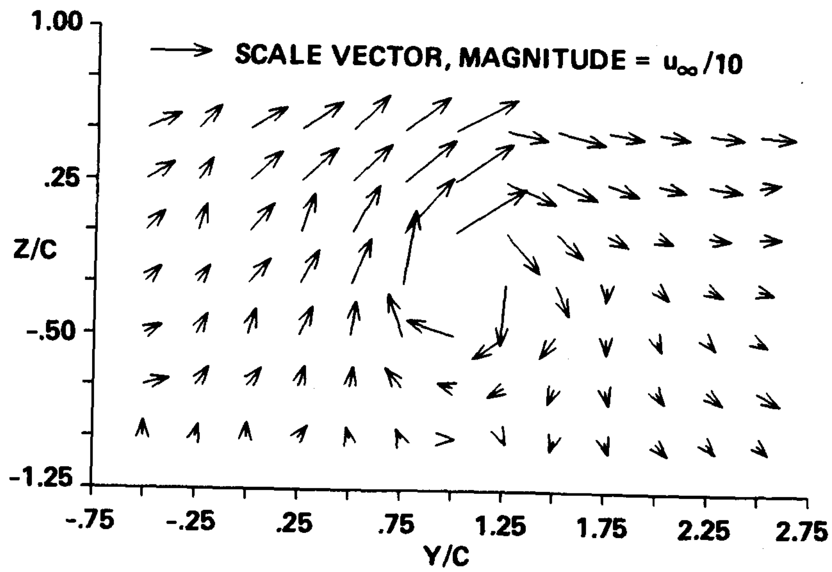

Figure 8. Large velocity grid data, configuration 4.

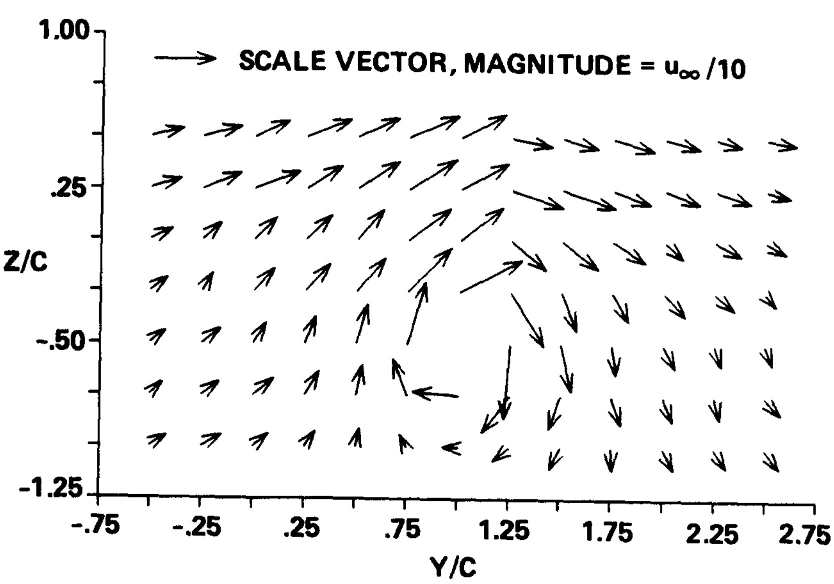

Figure 9. Large velocity grid data, configuration 5.

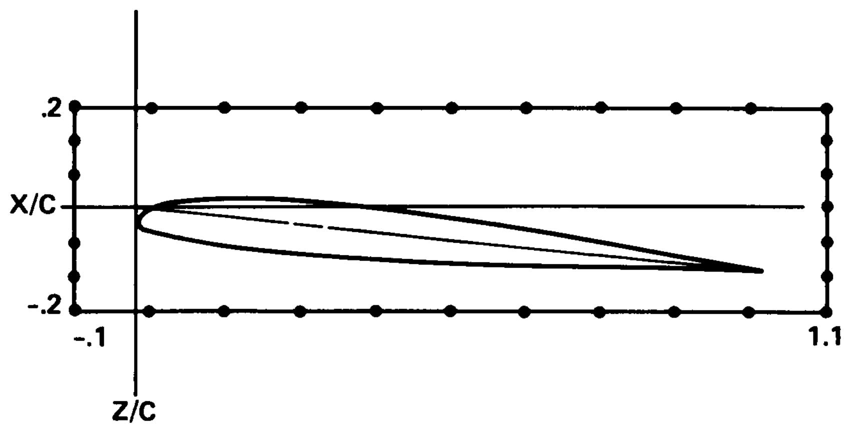

Figure 10. Circulation box geometry.

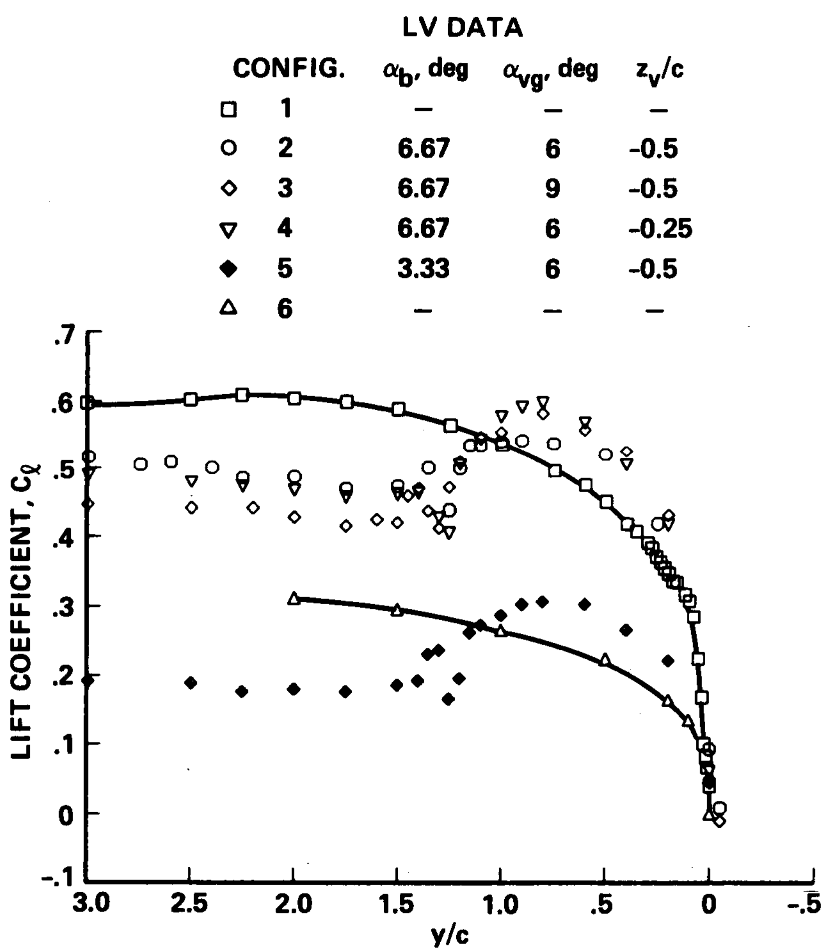

Figure 11. Lift distributions measured by the method of circulation.

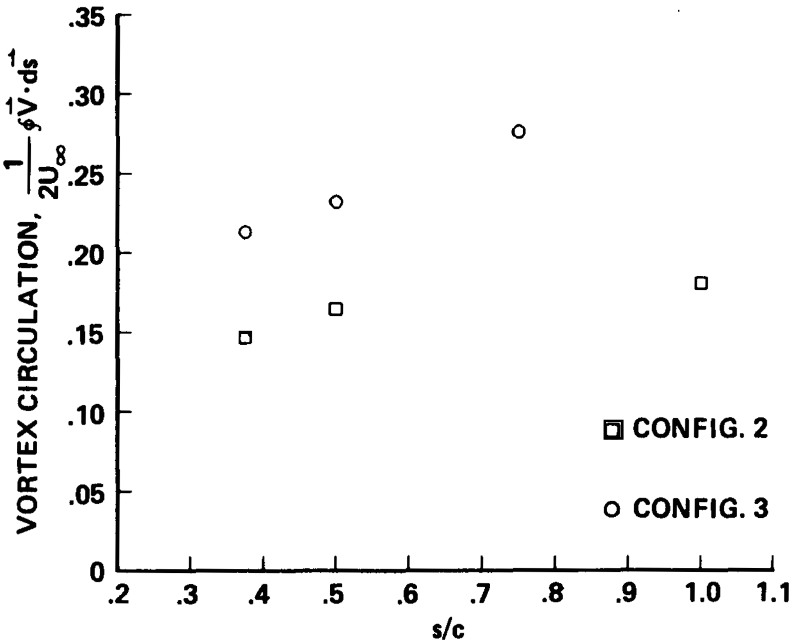

Figure 12. Vortex strength measured by the method of circulation.

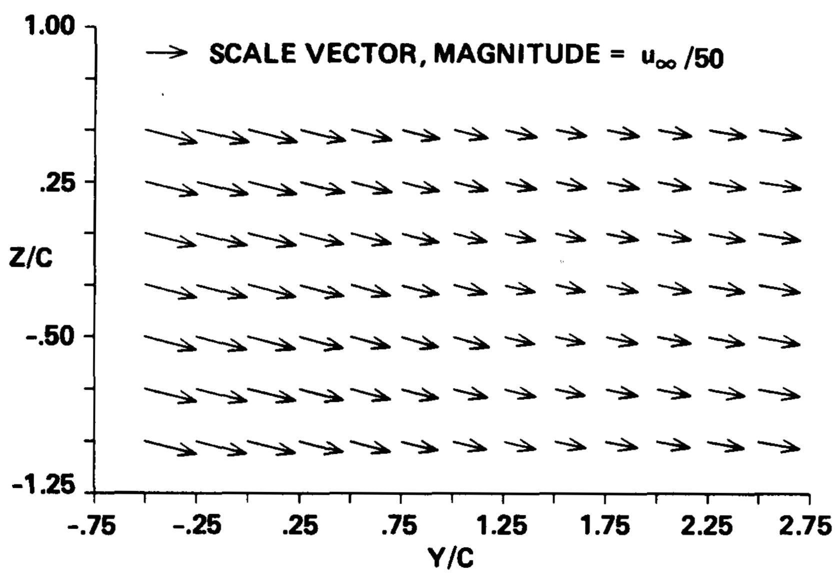

Figure 13. Calibration drift error for configuration 2.

Report Documentation Page

1. Report No.	2. Government Accession No.	3. Recipient's Catalog No.
NASA TM 100013		

4. Title and Subtitle	5. Report Date
Lift Distribution of Velocity Field Measurements for a Three-Dimensional, Steady Blade/Vortex Interaction	November 1987
	6. Performing Organization Code
7. Author(s)	8. Performing Organization Report No.
Stephen E. Dunagan and Thomas R. Norman	A-87306
	10. Work Unit No.
9. Performing Organization Name and Address	505-61-51
Ames Research Center Moffett Field, CA 94035	11. Contract or Grant No.
	13. Type of Report and Period Covered
12. Sponsoring Agency Name and Address	Technical Memorandum
National Aeronautics and Space Administration Washington, DC 20546-0001	14. Sponsoring Agency Code

15. Supplementary Notes

Point of Contact: Stephen E. Dunagan, Ames Research Center, MS T031, Moffett Field, CA 94035 (415)694-5043 or FTS 464-5043

16. Abstract

A wind tunnel experiment simulating a steady three-dimensional helicoptor rotor blade/vortex interaction is reported. The experimental configuration consisted of a vertical semispan vortex-generating wing, mounted upstream of a horizontal semispan rotor blade airfoil. A three-dimensional laser velocimeter was used to measure the velocity field in the region of the blade. Sectional lift coefficients were calculated by integrating the velocity field to obtain the bound vorticity. Total lift values, obtained by using an internal strain-gauge balance, verified the laser velocimeter data. Parametric variations of vortex strength, rotor blade angle of attack, and vortex position relative to the rotor blade were explored. These data are reported herein (with attention to experimental limitations) to provide a dataset for the validation of analytical work.

17. Key Words (Suggested by Author(s))	18. Distribution Statement
Rotary wings, Vortices, Blade-vortex interactions, Three-dimensional flow, Lift distributions, Helicopters, Interactional aerodynamics, Steady flow, Subsonic flow	Unclassified-Unlimited Subject Category - 02

19. Security Classif. (of this report)	20. Security Classif. (of this page)	21. No. of pages	22. Price
Unclassified	Unclassified	38	A03